DEUTSCHES ELEKTRONEN-SYNCHROTRON **DESY**

DESY 86-018
February 1986

PHYSICS AT LEP AT HIGH ENERGIES

by

G. Barbiellini
CERN – Geneva

M. Davier
Laboratoire de l'Accélérateur Linéaire, Orsay

K. Hagiwara, R.D. Peccei, F. Schrempp, D. Zeppenfeld
Deutsches Elektronen-Synchrotron DESY, Hamburg

H.U. Martyn
Rhein.-Westf. Tech. Hochschule, Aachen

B. Schrempp
Universität Hamburg

S. Yamada
University of Tokyo

ISSN 0418-9833

NOTKESTRASSE 85 · 2 HAMBURG 52

To be sure that your preprints are promptly included in the
HIGH ENERGY PHYSICS INDEX ,
send them to the following address (if possible by air mail) :

DESY
Bibliothek
Notkestrasse 85
2 Hamburg 52
Germany

DESY 86-018
February 1986

ISSN 0418-9833

PHYSICS AT LEP AT HIGH ENERGIES

G. Barbiellini*, M. Davier**, K. Hagiwara+, H.U. Martyn++, R.D. Peccei+, B.Schrempp', F. Schrempp+, S. Yamada'' and D. Zeppenfeld+

ABSTRACT

We discuss some of the physics that is expected to emerge at LEP at high energy (LEP, Phase II). We concentrate in particular on the reaction $e^+e^- \to W^+W^-$ and examine various experimental distributions which provide good tests of the standard model - in particular of the three gauge vertex. A careful discussion is also given of means to determine the W-mass, to one part per mil at Lep II. The importance of W decays for a clean determination of the various weak mixing angles is also emphasized. Finally, some possible signals for compositeness, which can be investigated in high energy e^+e^- collisions, are detailed.

Presented by R. D. Peccei at the LEP Jamboree, CERN, March 19, 1985. To appear in the Proceedings of the Jamboree.

* CERN, Geneva, Switzerland
** LAL, Orsay, France
+ DESY, Hamburg, Fed. Rep. Germany
++ RWTH, Aachen, Fed. Rep. Germany
' Univ. Hamburg, Hamburg, Fed. Rep. Germany
'' Univ. Tokyo, Tokyo, Japan

INTRODUCTION

The large electron-positron collider LEP, now under construction at CERN, will have sufficient CM energy, in its initial stage, to explore the rich physics associated with Z-boson production. In a later stage the energy of LEP is supposed to be increased to nearly 100 GeV per beam, so as to be above threshold for producing W-pairs. The purpose of this report is to explore some of the physics associated with this second phase of LEP - LEP II. In the course of this study, it became evident to us that the physics potential of LEP II is considerable, of a level comparable, if not greater, to that of the initial stage of LEP. We hope that the readers of this report will share this feeling of enthusiasm.

For the purpose of this study we have assumed that LEP II will have a maximum beam energy of 100 GeV and a maximum luminosity $L_{max} = 5\times10^{31}cm^{-2}sec^{-1}$. These numbers appear to be reasonable expectations [1], although a higher luminosity may not be totally out of the question. In this report we will assume for the most part that $E_b = 100$ GeV and consider, as a desired goal, that LEP II will be able to provide a yearly integrated luminosity at this energy, of 500 pb^{-1}. On occasion, however, we shall also discuss the physics potentiality of a smaller yearly integrated luminosity of 100 pb^{-1}.

One of the most exciting possibilities of operating LEP at high energy is the crossing of new thresholds. We do not, however, consider new particle productions in detail here, as this subject has been exhaustively discussed by the "new particle" working group at the LEP Jamboree [2]. We concentrate instead on the unexplored and beautiful W physics that becomes available after crossing the threshold for W^+W^- production. In addition, we study the effects that might arise from a possible new level of structure of matter, below that of quarks and leptons. Opening up a new energy window allows better limits to be set on the elementarity of leptons and quarks or, more spectacularly, the discovery of yet another layer of matter.

In our discussion we have ignored the existence of new effects as background to standard model physics, like W^+W^- production. One should be aware that, if indeed new effects - like the discovery of supersymmetric partners of quarks and leptons - appear in the energy range of LEP II, then some of our considerations will need revision. In general, for standard model physics, new thresholds make life more difficult, but also more interesting!

I. The total cross section for $e^+e^- \to W^+W^-$

The process $e^+e^- \to W^+W^-$ is totally predicted by the standard Glashow Salam Weinberg SU(2) x U(1) electroweak theory [3]. To lowest order there are three graphs contributing to this reaction, as shown in Fig 1. The presence of the three gauge couplings γW^+W^- and $Z^0W^+W^-$ make this process particularly interesting, since they afford a direct test of the non-Abelian nature of the weak interactions. In fact, as will be discussed in more detail below, it is likely that these three gauge couplings will be only probed by LEP II, in the foreseable future.

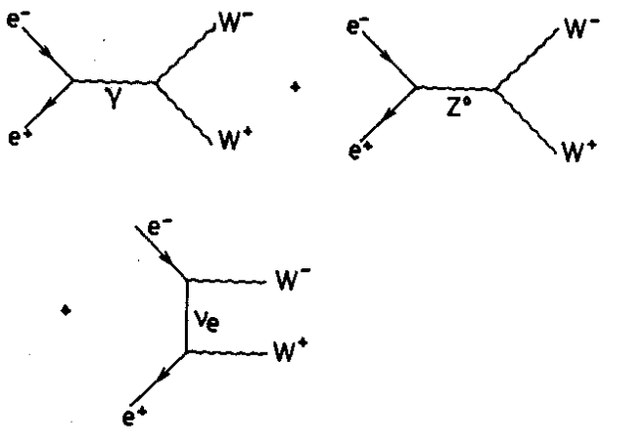

Fig 1: Lowest order contributions to the process $e^+e^- \to W^+W^-$

The total cross section for $e^+e^- \to W^+W^-$ in the standard model was computed, in lowest order, a decade ago [4] with the result:

$$\sigma = \frac{\pi\alpha^2\beta}{2\sin^4\theta_W s}\left\{\left[1 + \frac{2M_W^2}{s} + \frac{2M_W^4}{s^2}\right]\frac{1}{\beta}\ln\left(\frac{1+\beta}{1-\beta}\right) - \frac{5}{4}\right.$$

$$+ \frac{M_Z^2(1 - 2\sin^2\theta_W)}{(s - M_Z^2)}\left[2\left(\frac{M_W^4}{s^2} + 2\frac{M_W^2}{s}\right)\frac{1}{\beta}\ln\left(\frac{1+\beta}{1-\beta}\right) - \frac{s}{12M_W^2} - \frac{5}{3} - \frac{M_W^2}{s}\right]$$

$$\left. + \frac{M_Z^4(8\sin^4\theta_W - 4\sin^2\theta_W + 1)\beta^2}{48(s - M_Z^2)^2}\left[\frac{s^2}{M_W^4} + 20\frac{s}{M_W^2} + 12\right]\right\} \qquad (I.1)$$

Here $s = (2E_b)^2$ is the square of the CM energy and $\beta = (1 - \frac{4M_W^2}{s})^{1/2}$ is the W velocity.

Radiative corrections to this formula have been computed by Lemoine and Veltman [5] and Phillippe [6]. A number of remarks are in order:

i) The cross section is relatively big, around 20 pb at its peak. Furthermore, after a rapid threshold rise, it is approximately flat over the energy range of interest in LEP II. These features are clearly seen in Fig 2. Thus operating LEP II around E_b = 100 GeV one should obtain about 10^4 W^+W^- pairs per year, per intersection region, with an integrated yearly luminosity of 500 pb^{-1}. Even with a more conservative integrated luminosity of 100 pb^{-1}, the yearly yield of W^+W^- pairs (~ 2000) is substantial.

ii) The behavior of the $e^+e^- \to W^+W^-$ total cross section, shown in Fig 2, is crucially determined by gauge cancellations. The contribution of the ν-exchange graph alone in Fig 1, grows very rapidly with energy

$$\sigma_{\nu\text{-exch}} \underset{s>>M_W^2}{\simeq} \frac{\pi\alpha^2 s}{96\sin^4\theta_W M_W^4} \qquad (I.2)$$

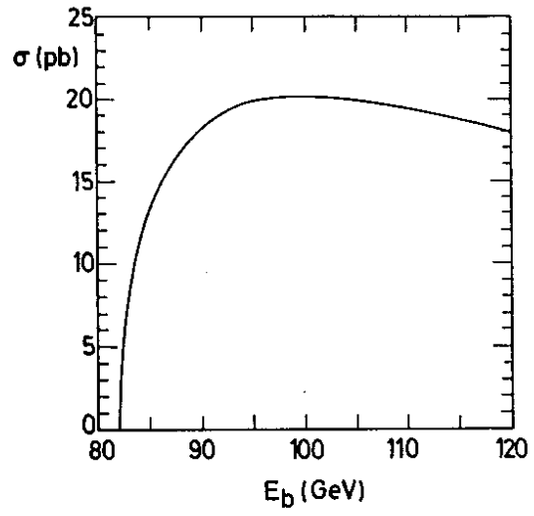

Fig 2: Total cross section for $e^+e^- \to W^+W^-$, as a function of the beam energy

and eventually violates unitarity. In the standard model the addition of the γ and Z^0 graphs, with coefficients dictated by gauge invariance, cancels this bad high energy behaviour, leading to a cross section which decreases with increasing energy:

$$\sigma_{GSW} \underset{s>>M^2_W}{\simeq} \frac{\pi\alpha^2}{2\sin^4\theta_W s} \ln\frac{s}{M^2_W} \qquad (I.3)$$

The contrast between the expectations due to pure υ-exchange and those of the standard model is shown pictorially in Fig 3. Although it would be easy to detect experimentally the difference between σ_υ and σ_{GSW} at LEP II, the direct measurement of the magnitude of $\sigma_{ToT}(e^+e^- \to W^+W^-)$ is unlikely to be the most sensitive test of <u>small</u> departures from the standard model. As will be discussed in the next section, measurements of the W differential cross section can provide more refined tests of the expectations of the theory. Furthermore, the absolute prediction for the magnitude of $\sigma_{ToT}(e^+e^- \to W^+W^-)$ necessitates the inclusion of radiative corrections. Roughly speaking, $\sigma_{ToT} \sim \sin^{-4}\theta_W$, and therefore it is clearly important to know what $\sin^2\theta_W$ should be used in the calculation. We shall return to this point also in Sec II.

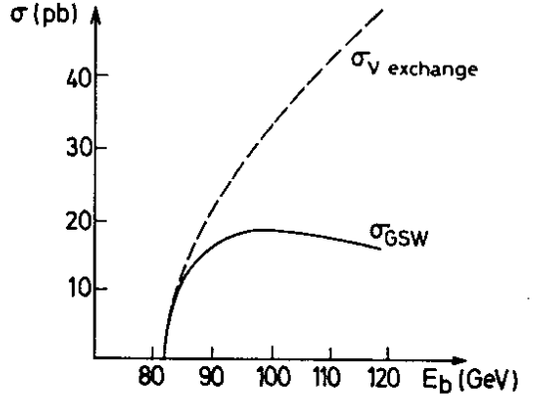

Fig 3: Comparison between the standard model expectations and those of pure υ-exchange

iii) The W^+W^- signal at LEP II can be easily seen in the 4 jet cross section, arising from both W's decaying into $\bar{q}q$ pairs. Roughly half of the total W^+W^- sample will contribute to the 4 jet cross section, so that, at E_b = 100 GeV, $\sigma_{4jet}(e^+e^- \to W^+W^-) \simeq$ 10 pb. This 4-jet signal has no significant background. From QCD one expects, of course, some 4 jet events, but their level is much lower: $\sigma^{QCD}_{4jet} \simeq \alpha_s^2\, \sigma(e^+e^- \to \text{hadrons}) \simeq$ 0.5 pb. We have estimated how much of this 4-jet cross section can be detected at LEP II, by putting in some reasonable cuts. Fig 4 gives the observed 4 jet cross section in the LEP II energy range , imposing a forward cut on the produced quarks (taken to be the same as jets for this calculation) $|\cos\theta_q| < 0.9$ and also an overlap cut between the jets $|\cos\theta_{ij}| < 0.9$. The process $e^+e^- \to W^+W^- \to q\bar{q}q\bar{q}$ was calculated using a Monte Carlo program kindly supplied to us by R. Kleiss [7], in which the W width is included. The more significant cut is by far the forward cut. However, the efficiency to detect 4 jets, as shown in Fig 5, appears to be roughly energy independent, and is at the level of 50-60 %. Prospects of collecting a clean and sizable W^+W^- sample at LEP II appear therefore excellent.

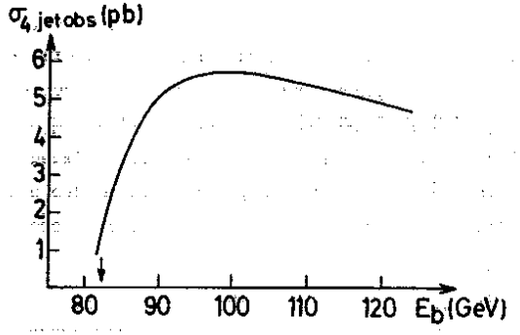

Fig 4: Estimate of the 4 jet cross section due to W^+W^-, observable at LEP II

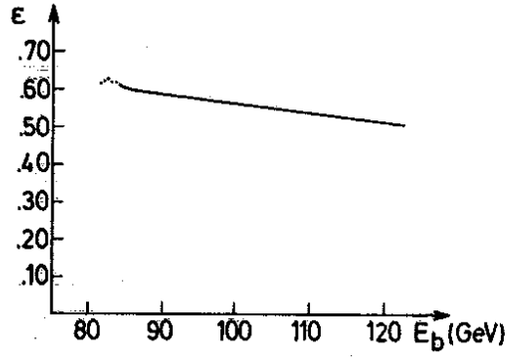

Fig 5: Efficiency to detect 4 jets, from W^+W^- hadronic decays

iv) As mentioned above, the W^+W^- signal into 4 jets is remarkably clean at LEP II. Furthermore, other channels in which one W decays hadronically and the other leptonically, or both decay leptonically, have equally clean signatures [2 jets + lepton + missing energy; 2 leptons + missing energy]. Thus with 10^4 W^+W^- pairs one should really be able to do detailed investigations of the W production and decay properties. This is important because LEP II is probably the only place where the 3-gauge vertex, particularly the $Z^0W^+W^-$ vertex, can really be studied. W pairs can, of course, also be produced at hadronic colliders through $q\bar{q} \to W^+W^-$ annihilation. However, the detection of this process is very hard. At the $Sp\bar{p}S$ collider, at $\sqrt{s}$ = 630 GeV, W^+W^- production is hopelessly small. At the Tevatron, however, since $\sqrt{s}$ = 2 TeV one can estimate [8] that $\sigma(p\bar{p} \to W^+W^-X) \approx 10$ pb. Nevertheless, because the integrated luminosity per

year at the Tevatron is supposed to be only in the range of 10-50 pb^{-1}, the number of W-pairs produced is likely to be at least an order of magnitude less than at LEP II. Furthermore, it will be nearly impossible to disentangle this signal from the background produced by processes like $p\bar{p} \to W$ + 2 jets, etc., which have large cross sections at the Tevatron [8]. The situation may be a little better at hadronic supercolliders operating at $\sqrt{s}$ = 20-40 Tev. there , even after rapidity cuts, the W^+W^- production is large [9], $\sigma^{W^+W^-} \sim$ (50 - 100)pb, and the integrated yearly luminosity should be in the range of 10^3 -10^4 pb^{-1}. Hence 10^6 W^+W^- pairs could be produced per year, which might allow the extraction of the $q\bar{q} \to W^+W^-$ signal from the background. It is clear, however, that LEP II is the place to do detailed tests of the three gauge vertex [10].

II. The angular distribution for $e^+e^- \to W^+W^-$

With the expected yearly sample of events at LEP II it should be quite feasible to study in detail the angular distribution of the produced W's. This will allow a separation of the different helicity contributions (Sect. IIa) and will give more careful checks on the three gauge couplings than can be afforded by just a total cross section study (Sect. IIb).

The expression for the W angular distribution has been calculated, in lowest order, in Ref [4] with the result:

$$\frac{d\sigma}{d\Omega} = \frac{\alpha^2\beta}{32\sin^4\theta_W s}\left\{ F_1(\theta,s) + \left[\sin^4\theta_W + \frac{\sin^2\theta_W(1 - 4\sin^2\theta_W)s}{2(s - M_Z^2)} + \frac{(8\sin^4\theta_W - 4\sin^2\theta_W + 1)s^2}{8(s - M_Z^2)^2} \right] F_2(\theta,s) + \left[\frac{(2\sin^2\theta_W - 1)s}{2(s - M_Z^2)} - \sin^2\theta_W \right] F_3(\theta,s) \right\} \qquad \text{(II.1)}$$

where the functions $F_i(\theta,s)$ (i=1,2,3) are given by:

$$F_1(\theta,s) = 2\left(\frac{s}{M_W^2}\right) + \frac{1}{2}\beta^2\sin^2\theta\left\{\left(\frac{s}{t}\right)^2 + \frac{1}{4}\left(\frac{s}{M_W^2}\right)^2\right\} \qquad \text{(II.2a)}$$

$$F_2(\theta,s) = \beta^2\left\{16\left(\frac{s}{M_W^2}\right) + \left[\left(\frac{s}{M_W^2}\right)^2 - 4\left(\frac{s}{M_W^2}\right) + 12\right]\sin^2\theta\right\} \qquad \text{(II.2b)}$$

$$F_3(\theta,s) = 16\left(1 + \frac{M_W^2}{t}\right) + 8\beta^2\left(\frac{s}{M_W^2}\right) + \frac{\beta^2}{2}\sin^2\theta\left[\left(\frac{s}{M_W^2}\right)^2 - 2\left(\frac{s}{M_W^2}\right) - 4\left(\frac{s}{t}\right)\right] \qquad \text{(II.2c)}$$

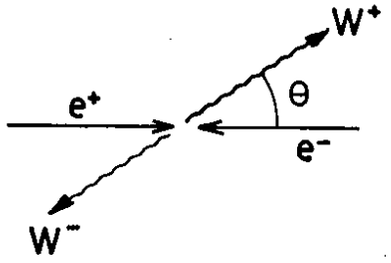

Fig 6: Definition of the angle θ

Here t is the momentum transfer

$$t = M_W^2 - \frac{1}{2}s + \frac{1}{2}\beta s\cos\theta \qquad \text{(II.3)}$$

and θ is the angle between the produced W^+ and the direction of the incoming positron, as shown in Fig 6. This differential cross section is plotted in Fig 7 for two values of E_b . As can be seen from the

figure, the angular distributions are forward peaked. That is, the distributions are peaked along the initial charge direction, with the W^+ preferentially being emitted along the initial e^+ direction. This forward peaking increases as the beam energy increases. One can understand both of these qualitative features very easily. They arise essentially due to the influence of the ν-exchange graph in Fig.1. The $\frac{1}{t}$ neutrino propagator drives the produced W's along the initial charge direction and the influence of this pole is more pronounced as the energy increases.

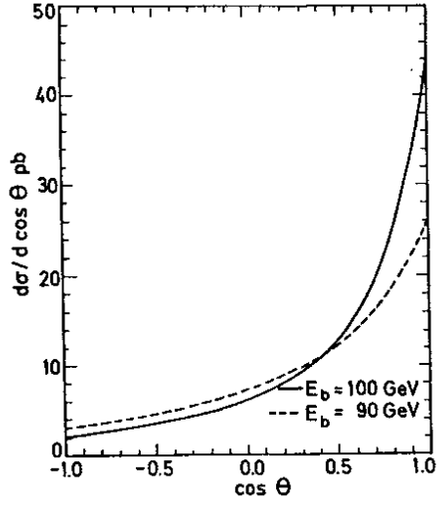

Fig 7: Angular distribution of the produced W^+, for two beam energies

IIa) Helicity Properties of W Production

The W-pairs produced in e^+e^- collisions have characteristic helicity patterns which reflect the (V-A) nature of the W coupling to leptons. In particular, because here one is producing a $W^+ W^-$ pair and not just a single W, like in the case of hadronic colliders, a sizable fraction of the produced W's will be longitudinally polarized. This is particularly interesting since the existence of a longitudinally polarized W is intimately connected with the mechanism of W-mass

generation (Higgs mechanism). As is well known, a massless spin 1 particle has only transverse polarizations ($\lambda = \pm 1$). A massive spin 1 particle has also a longitudinal polarization ($\lambda = \pm 1, 0$). Thus LEP II offers the possibility to study longitudinally polarized W bosons and thereby provides a window into the Higgs mechanism.

One can give a simple qualitative discussion of why one expects longitudinally polarized W's to be produced in the process $e^+e^- \to W^+ W^-$. For orientation, first look at single W production in hadronic collisions. The V-A form of the interaction which gives the process $d\bar{u} \to W^-$ fixes the quark helicities, as shown in Fig 8a. The produced W^- will thus have helicity $\lambda = +1$, if it is produced along the $\bar{u}$ direction (as shown in Fig 8b), or helicity $\lambda = -1$, if it is produced along the d direction. Clearly, however, no longitudinally polarized W^- are produced in this way.

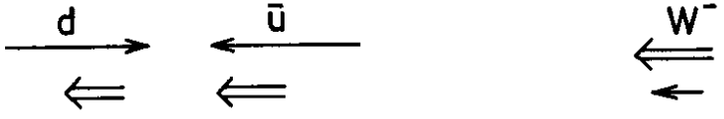

Fig 8: a) Quark helicities in $d\bar{u} \to W^-$ b) W^- helicities in $d\bar{u} \to W^-$

The situation for the process $e^+e^- \to W^+W^-$ is different. Because one is dealing with vector or axial vector interactions, in the limit of negligible electron mass, scattering will only occur if the helicities of the initial leptons are opposite. That is $\sigma_{LL} = \sigma_{RR} = 0$. Because of the V-A form of the $e\nu W$ vertex, the ν-exchange graph will only contribute if the initial e^- is left handed and the e^+ is right handed. This σ_{LR} cross section, in fact, dominates over the σ_{RL} cross section. This can be understood as follows. At LEP II energies, the Z^0 mass starts being unimportant. Thus, instead of γ and Z^0 exchange one can think in terms of W_3 and B (the hypercharge gauge boson) exchange. W_3 contributes only to σ_{LR} and cancels part of the ν exchange contribution to this cross section. The hypercharge gauge boson, which could

contribute to σ_{RL} does not, in fact, since it does not couple to $W^\pm$. Hence at LEP II γ and Z graphs in σ_{RL} nearly cancel and one finds that $\sigma_{RL} \sim 10^{-2}\, \sigma_{LR}$. Therefore, for all practical purposes, the dominant helicity configuration for the process $e^+e^- \to W^+W^-$ is that shown in Fig. 9. Recall, however, that the differential cross section for W production is very forward peaked. In the forward direction the process $e^+e^- \to W^+W^-$ can be represented by Fig 10. Since the total W^+W^- spins must add to unity we expect, therefore, the dominant helicity contributions to be:

$$W^+(\lambda = +1),\ W^-(\lambda = 0) \quad \text{or} \quad W^+(\lambda = 0),\ W^-(\lambda = -1) \qquad \text{(II.4)}$$

which substantiates our contention that a significant fraction of the W bosons produced in $e^+e^- \to W^+W^-$ are longitudinally polarized. Actually, as we will discuss below, the configuration of Eq. (II.4) only dominate near $\theta = 0$.

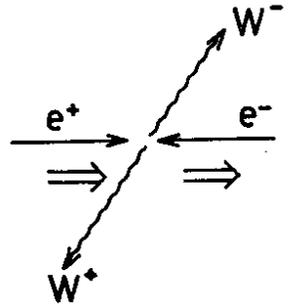

Fig 9: Dominant helicity configurations of the e^+ and e^-

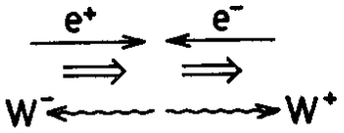

Fig 10: Helicity structure for $e^+e^- \to W^+W^-$ in the forward direction

Cabibbo and Gatto [11], in a seminal paper nearly a quarter of a century ago, studied the production of polarized spin 1 particles in e^+e^- collisions. Of course, high energies for them were energies of the order of a few GeV, but their general phenomenological analysis still applies. More recently, Gaemers and Gounaris [12] have analyzed the process $e^+e^- \to W^+W^-$ for arbitrary polarization in the initial and final state. In their calculation Gaemers and Gounaris computed the contribution of the graphs in Fig 1 where, however, the three gauge vertices $\gamma\, W^+W^-$ and $Z^0\, W^+W^-$ are allowed to take the most general

form consistent with Lorentz invariance. To make this report self contained, we have reproduced in Appendix A the general formulas of Gaemers and Gounaris in a format more convenient for our purposes.

Restricting ourselves for the moment to the case in which the three gauge vertices are given by the standard electroweak model values, we display in Figs 11 and 12 the differential cross section for producing polarized W bosons in e^+e^- collisions, at two different beam energies. What is plotted in these figures are the distributions in which both W come out transversly polarized (TT) or both come out longitudinally polarized (LL) or one W is longitudinally and the other is transversly polarized (TL+LT). Near threshold for W production, Fig. 11, the percentage of W bosons which are longitudinally polarized is greater, and less forward peaked, than near the cross section maximum, Fig. 12. For instance, for E_b = 84 GeV and at cos θ = 0.85 the relevant percentages are 46 % TT, 36 % TL + LT and 18 % LL. At E_b = 100 GeV and at cos θ = 0.90 these percentages have altered to 70 % TT, 20 % TL + LT and only 10 % LL. Of course, in the forward and backward region the amplitude for TL + LT is the total amplitude, because of the arguments given earlier.

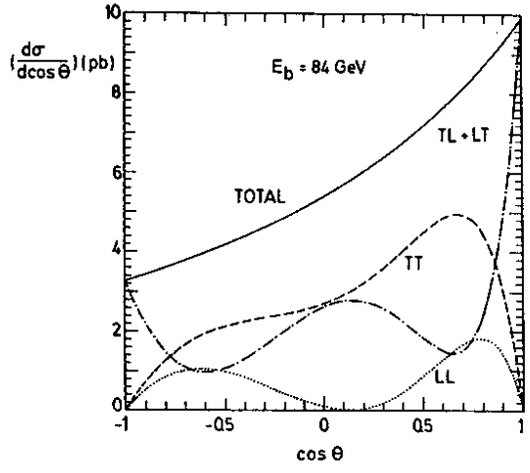

Fig 11: Differential cross section for producing polarized W bosons in e^+e^- collisions, near threshold

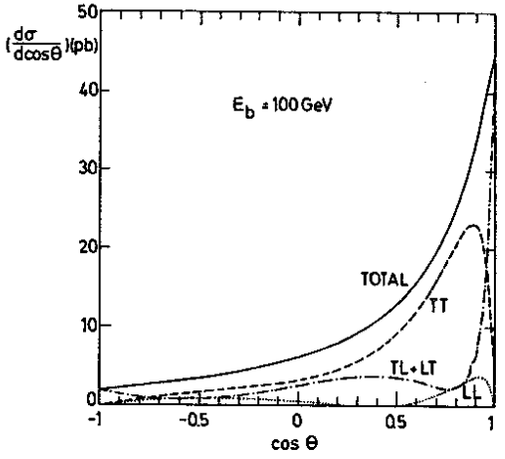

Fig 12: Differential cross section for producing polarized W bosons in e^+e^- collisions, near the cross section maximum

The qualitative trends of these figures can be readily understood from the formulas in Appendix A. The principal angular dependence is governed by the neutrino exchange graph. Thus, for instance, the maximum of the TT distribution will roughly occur at an angle θ_{max} where C_{-+} (see Eq (A17)) is a maximum. This angle is approximately given by

$$1 - \cos\theta_{max} \simeq \frac{(1-\beta)^2}{2} \qquad \text{(II.5)}$$

Similarly, one can compute that the half width of the TL+LT curve occurs at, approximately,

$$1 - \cos\theta_{1/2} \simeq \frac{\sqrt{2}-1}{2}(1-\beta)^2 \qquad \text{(II.6)}$$

In principle, one can study separately the cross section for transversly and longitudinally polarized W bosons by using the angular distribution of the decay products as an analyzer [11]. What one would ideally like to study really is the cross section for producing two longitudinally polarized W's. As we commented

earlier the presence of W_{long} most clearly reflects the $SU(2)xU(1) \to U_{em}(1)$ breakdown. In fact, it has been argued that in the case of a strongly interacting Higgs sector, two longitudinal W bosons are expected to suffer a strong rescattering [13]. This is schematically indicated in Fig 13 and could lead to additional contributions to the LL cross section, besides those shown in the figures. Unfortunately, it is unlikely that these strong rescattering contributions can be felt near the threshold of $e^+e^- \to W^+W^-$. Furthermore, since the LL cross section is itself rather small, any variations of it are going to be very hard to detect.

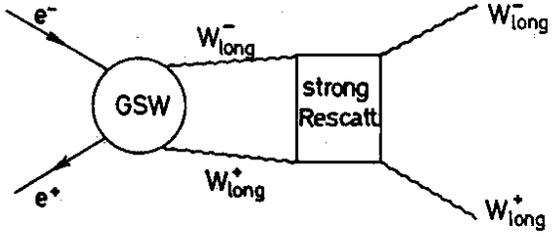

Fig 13: Strong rescattering correction to W_{long} production

As a means to increase statistics, it may be useful to study the inclusive cross section for producing a W boson of a given polarisation, irrespective of what the polarisation of the other boson is. In such a measurement, it is convenient to add together the angular distributions for both W^+ and W^-, so as to avoid determining the charge of the byproducts. These inclusive distributions are then symmetric in θ, and because one sums over both W^+ and W^- events one has

$$\int_{-1}^{1} \left[\frac{d\sigma_L}{d\cos\theta} + \frac{d\sigma_T}{d\cos\theta} \right] d\cos\theta = 2\sigma_{TOT}\ (e^+e^- \to W^+W^-) \qquad (II.7)$$

In Fig 14 we present the expected angular distributions for $\frac{d\sigma_L}{d\cos\theta}$ and $\frac{d\sigma_T}{d\cos\theta}$ at E_b = 100 GeV in the standard model. Here θ is the angle of the emitted W with respect to the e^+e^- collision axis. Note that although σ_L is smaller than σ_T, it is by no means negligible. The equality of σ_L and σ_T at $\theta = 0, \pi$ follows again simply by angular momentum conservation. We have detailed in Appendix B, using again the general formulas of Appendix A, the predictions for $\frac{d\sigma_{L,T}}{d\cos\theta}$ in the standard model.

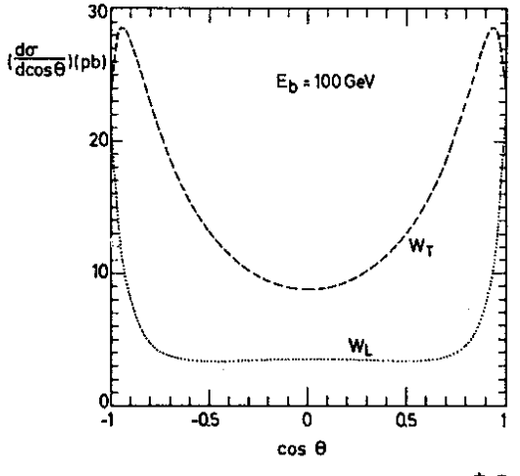

Fig 14: Angular distributions of polarized W's in e^+e^- collisions

Not having to determine the charge of the W's is an advantage, since it means that these angular distributions can in principle be reconstructed by using essentially all events. (For the doubly leptonic decays there is a two-fold ambiguity). This is in contrast to the case of the ordinary $W^\pm$ angular distributions, where there is a problem using all the W decays, including the 4 jet events, to measure the angular distribution. The reason is that particles emitted at low rapidity in the W rest frame will spoil the charge determination of the two W's. This will bias the angular distribution, which is very asymmetric. Also the QCD 4-jet background, although negligible for the total rate, will affect the angular distribution. Thus it is safer to use only events where at least one W decays leptonically to measure the $W^\pm$ angular distribution. At

any rate, to obtain $\frac{d\sigma_{L,T}}{dcos\theta}$ what one needs to do is to determine the W axis kinematically, which can be done since one knows that the W energy is just E_b. Having determined the W axis one can boost back the W decay products (jet jet or lν) to the W CM frame. In this frame, the angular distribution of the decay products with respect to the W axis has a simple form which depends on the helicity of the W. Let θ^* be the angle between the W axis and the decay products in the W CM frame, as shown schematically in Fig 15.

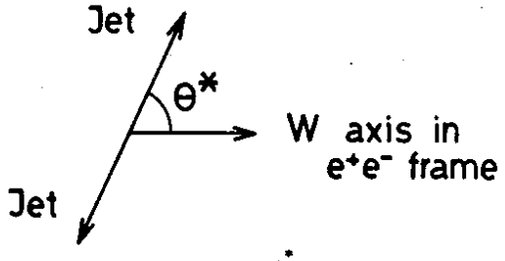

Fig 15: Definition of the angle θ^*

If the W is transversly polarized then the distribution of the decay products is proportional to $(1 + \cos^2\theta^*)$. This result is just the sum of the familiar $(1 \pm \cos\theta^*)^2$ distributions of particles and antiparticles in (V-A)interactions. On the other hand, if the W is longitudinally polarized, the distribution of the decay products has to vanish along the W axis and a simple calculation shows that it is proportional to $\sin^2\theta^*$. Hence, the measurement of the double differential cross section

$$\frac{d\sigma}{dcos\theta dcos\theta^*} = \frac{3}{4}\sin^2\theta^* \left(\frac{d\sigma_L}{dcos\theta}\right) + \frac{3}{8}[1 + \cos^2\theta^*]\left(\frac{d\sigma_T}{dcos\theta}\right) \qquad (II.8)$$

allows the experimental extraction of the polarized differential cross sections $\frac{d\sigma_L}{dcos\theta}$, $\frac{d\sigma_T}{dcos\theta}$.

II b) Checking the three gauge vertex

A careful study of the differential angular distribution of the produced W bosons at LEP II can provide a rather stringent test of the form of the three gauge vertex. As discussed in more detail in Appendix A, the three boson vertices shown in Fig 16, depend in general on seven form factors.

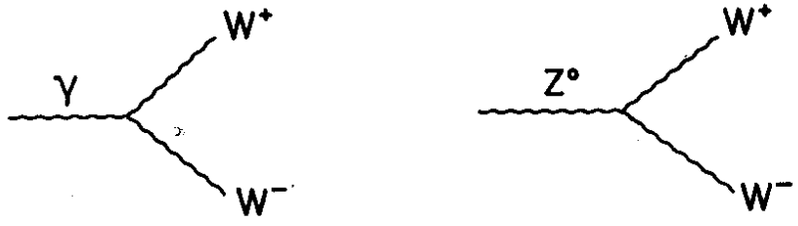

Fig 16: γW^+W^- and $Z^0W^+W^-$ three boson vertices

Imposing C, P and T reduces the number of form factors to three. These three form factors for the photon case, in the static limit, just describe the charge, magnetic dipole moment and electric quadrupole moment of the W. We shall assume, in what follows, that there will not be large momentum transfer dependence of these form factors in the LEP II energy region. Therefore we shall effectively restrict ourselves to a static parametrization for the three boson vertices. For the photon case this reads [12]

$$\Gamma^{\gamma}_{\mu\alpha\beta}(p,q_1,q_2) = ieg_{\gamma WW}\Big\{(q_2 - q_1)_\mu\left[\left(1 + \frac{\lambda_\gamma p^2}{2M_W^2}\right)g_{\alpha\beta} - \lambda_\gamma\frac{p_\alpha p_\beta}{M_W^2}\right]$$

$$+ (p_\beta g_{\mu\alpha} - p_\alpha g_{\mu\beta})[1 + \kappa_\gamma + \lambda_\gamma]\Big\} \qquad (II.9)$$

For the $Z^0W^+W^-$ vertex, one has an analogous expression with the replacements

$$g_{\gamma WW} \leftrightarrow g_{ZWW} \; ; \; \lambda_\gamma \leftrightarrow \lambda_Z \; ; \; \kappa_\gamma \leftrightarrow \kappa_Z \qquad \text{(II.10)}$$

The unit charge of the W^+ implies that

$$g_{\gamma WW} = 1 \qquad \text{(II.11)}$$

The W dipole and quadrupole moments are functions of κ_γ and λ_γ and are given by

$$\mu_\gamma = \frac{e}{2M_W} [\, 1 + \kappa_\gamma + \lambda_\gamma \,] \qquad \text{(II.12a)}$$

$$Q_\gamma = - \frac{e}{M^2_W} [\, \kappa_\gamma - \lambda_\gamma \,] \qquad \text{(II.12b)}$$

In the standard model [3] one has

$$g_{ZWW} = \cot\theta_W \; ; \; \kappa_\gamma = \kappa_Z = 1 \; ; \; \lambda_\gamma = \lambda_Z = 0 \qquad \text{(II.13)}$$

LEP II can test for departures of the above parameters from the standard model values [14]. Although one can let, in principle, all parameters vary, for illustrative purposes it is better to only let one parameter vary at the time. In what follows we will consider, therefore, what is the effect of keeping $\kappa = \kappa_\gamma = \kappa_z$ arbitrary, fixing the rest of the constants in the three boson vertex to their standard model values. Qualitatively, as Figs 17 and 18 show, the effect of having $\kappa > 1$ is to increase the forward peaking in the W angular distribution. The effect of $\kappa < 1$, in contrast, is to give a larger backward tail. Both effects become more pronounced as the energy increases.

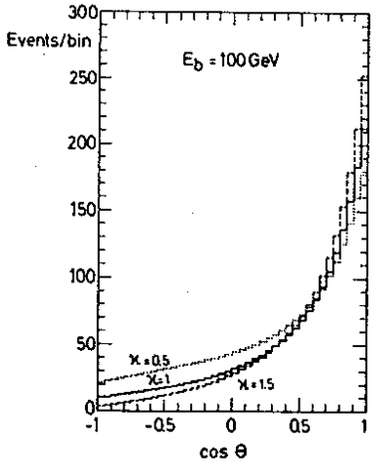

Fig 17: W angular distribution, for various κ, at E_b = 100 GeV

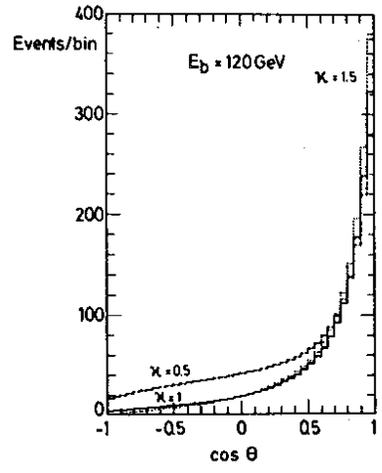

Fig 18: W angular distribution, for various κ, at E_b = 120 GeV

To display the above trends in a better way, we have plotted the ratio R of the differential angular distribution for $\kappa \neq 1$ to that in the standard model:

$$R = \frac{\left(\frac{d\sigma}{dcos\theta}\right)_\kappa}{\left(\frac{d\sigma}{dcos\theta}\right)_{GSW}} \qquad \text{(II.14)}$$

Figs 19 and 20 show the statistical errors that 2000 W^+W^- events, at E_b= 100 GeV, would give for R for the cases in which κ = 1.5, and κ = 0.5, respectively. Clearly, we see that with this many W pairs it is quite easy to distinguish κ = 1.5 or κ = 0.5 from κ = 1. Nominally, this number of events are what is produced in a run of 100 pb^{-1}. However, as we mentioned earlier, to do precise tests of the W angular distribution one needs to make sure of the W charge determination. Hence, one should probably only use events in which one W decays leptonically, which reduces the number of events by 50 % (or more, considering detection efficiencies).

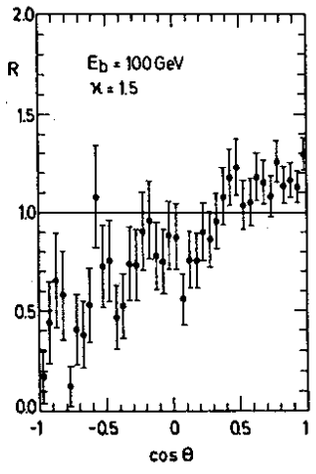

Fig 19: statistical errors on R for κ = 1.5

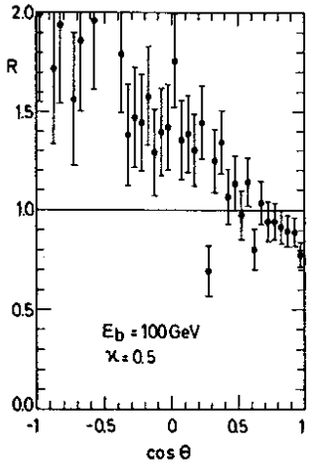

Fig 20: statistical errors on R for κ = 0.5

More quantitatively, one can ask for the allowed range in κ, to three standard deviations, which can be determined from a given number of events. In Fig 21 we show χ^2 curves for κ for the specific case of 2000 and 4000 W^+W^- events. We see from this figure that a measurement of κ to the 10 % level is achievable at LEP II, if one collects 500 pb^{-1}. Probably 50 pb^{-1} should suffice for a 50 % measurement of κ. There are, of course, other ways to study deviations of the three boson coupling from the standard model values, besides those involving the detailed study of the W angular distributions. For instance, recently Dicus and Kallianpur [15] have suggested that a nice quantity to study for these purposes is the electron energy spectrum in $W \to e\nu$ decays.

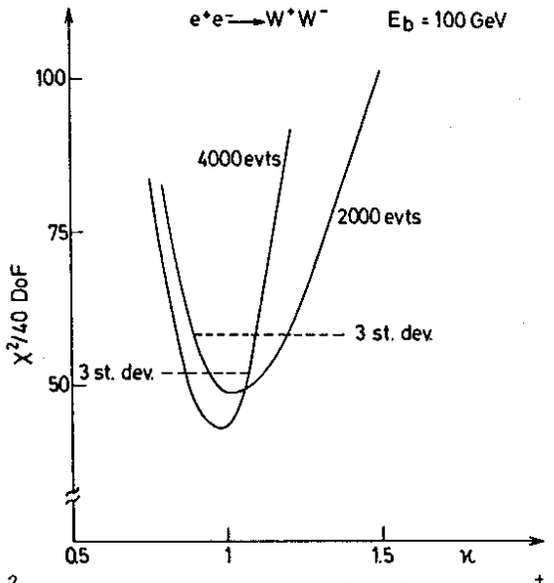

Fig 21: χ^2 curves for κ, for the case of 2000 and 4000 W^+W^- events

The differential cross section $d\sigma/dE_e$, where E_e is the electron energy, is sensitive to κ, and the sensitivity increases with beam energy, E_b . It does not appear, however, that a study of this quantity can quite compare in accuracy to that coming from a study of R. This matter has been investigated in some detail by Bilal and Davier [16], in a Monte Carlo study which included some realistic acceptance cuts. Fig 22 shows the ratio of the expected cross section for $\kappa \neq 1$ to that of the standard model, as a function of E_b . The error bars correspond to what might be expected in a run of 100 pb^{-1} at a beam energy of 110 GeV. (Since the effect of $\kappa \neq 1$ increases with E_b , it is obviously better to operate at the highest possible beam energy, although E_b = 110 GeV might not be achievable at LEP II)

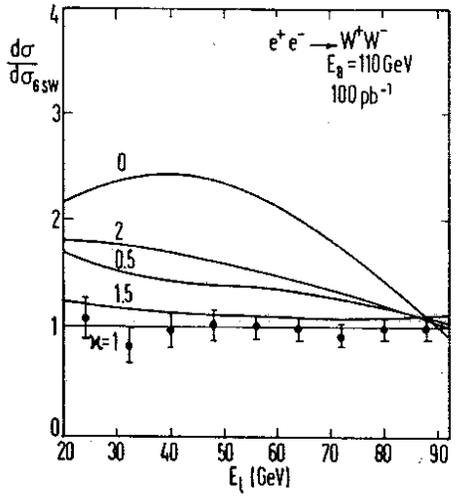

Fig 22: Expectations for the ratio $d\sigma/d\sigma_{GSW}$ versus E_e , for various values of κ. The error bars correspond to a run of 100 pb^{-1} at E_b = 110 GeV

The sensitivity of the measurement of this distribution to the parameter κ is characterized by the range $0.78 < \kappa < 1.47$, assuming 100 pb^{-1} at E_b = 110 GeV. In contrast a measurement of R, using the same cuts and assumptions, restricts κ to the range $0.85 < \kappa < 1.34$ [16]. Hence, as we indicated, the measurement of the W angular distribution is more sensitive to possible departures from the standard model.

Looking for variations produced by non standard gauge couplings, raises the parallel question of how well can LEP II measure the effects of radiative corrections in $e^+e^- \to W^+W^-$. We are not able to give a quantitative answer to this question at the moment, since it would require a thorough reanalysis of the angular dependence of the corrections for a fixed set of input parameters. The existing calculations [5] [6] only present their results for some selected energies and parameters and are not immediately useful. This is not surprising, since these calculations were all done previous to the discovery of the W and Z and thus, for example, normalize $\sin^2\theta_W$ in a way which is not particularly convenient. This matter is presently under investigation and it may be that one may yet find some particularly sensitive test.

However, from the existing calculations this appears to be unlikely. For instance, at E_b = 100 GeV, Fig 23, taken from Ref [5], shows the ratio of the first order to lowest order differential cross section as a function of the W scattering angle, for three values of the Higgs mass. As can be seen, unfortunately, the correction is biggest precisely in the region where the cross section itself is smallest!

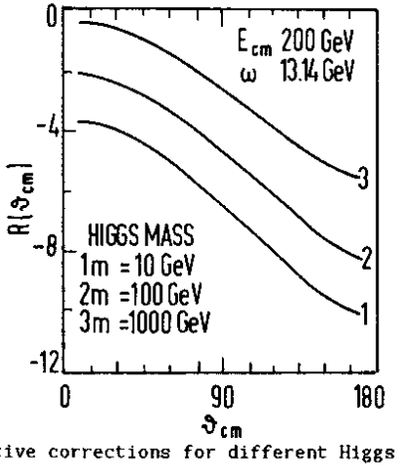

Fig 23: Percentage change of radiative corrections for different Higgs masses, from Ref [5]. (ω is the photon cut off energy)

III PROPERTIES OF W BOSONS

We mentioned earlier that one of the unique features of LEP II is its capability of producing a clean sample of W events, with negligible background. This will make it possible to study some of the detailed properties of the W bosons, most notably their mass and decay branching fractions.

III.1 Theoretical significance of a precise W Mass Measurement

A careful measurement of the W mass will provide a rather stringent test of the validity of the standard model, beyond leading order. As is well known, the lowest order formula for the W mass

$$M^2_W = \frac{\pi\alpha}{\sqrt{2}G_F \sin^2\theta_W} \qquad \text{(III.1)}$$

gets modified by radiative corrections. The resulting formula for M^2_W is simplest if one uses a definition for the Weinberg angle directly related to the physical W and Z masses themselves [17]. Namely,

$$\sin^2\theta_W = 1 - M^2_W / M^2_Z \qquad \text{(III.2)}$$

Then one finds for M^2_W the formula [18]:

$$M^2_W = \frac{\pi\alpha}{\sqrt{2}G_\mu[1 - M^2_W/M^2_Z][1 - \Delta r]} \qquad \text{(III.3)}$$

Here α is the fine structure constant $\alpha = \alpha(0)$, evaluated at zero momentum transfer. G_μ is the Fermi constant obtained from μ decay, in which certain photonic radiative corrections are included [19]. Numerically one has

$$G_\mu = (1.16637 \pm 0.00002)\times 10^{-5}\ \text{GeV}^{-2} \qquad \text{(III.4)}$$

The quantity Δr can be computed theoretically [18] and is rather large (~ 0.07). Its origin comes mostly from the running of α, from its static value to the scale of M_W [20]. That is, approximately,

$$\frac{\alpha}{1-\Delta r} \simeq \alpha(M^2_W) \simeq \frac{1}{128} \qquad \text{(III.5)}$$

The exact value of Δr depends weakly on the mass value for the Higgs boson. Taking $m_H = M_Z$ and assuming that $m_t = 36$ GeV, one finds numerically that [18]

$$1 - \Delta r = 0.9304 \pm 0.0020 \qquad \text{(III.6)}$$

The error in the above determination comes from uncertainties in the vacuum polarization contributions due to hadrons made up of light quarks. If $m_H \gg M_Z$, (III.6) gets an additional contribution, whose leading form reads

$$(\Delta r)_{\text{Higgs}} \simeq \frac{11\alpha}{48\pi\sin^2\theta_W} \ln\frac{m^2_H}{M^2_Z} \simeq 0.0024 \ln m^2_H/M^2_Z \qquad \text{(III.7)}$$

Thus a 1 TeV Higgs would change Δr from about 7% to about 6 %.

A precise determination of M_W, along with the precise value of the Z^0 mass, which one will surely obtain at LEP and SLC, will allow for a direct test of the theoretical shift Δr. Let us rewrite E_q (III.3) as

$$1 - \Delta r = \frac{\pi\alpha}{\sqrt{2}G_\mu M^2_W(1 - M^2_W/M^2_Z)} \qquad \text{(III.8)}$$

which expresses the radiative shift Δr entirely in terms of physically measurable quantities. Clearly, the experimental error in $1-\Delta r$ comes essentially only from the errors on the W and Z masses, as α and G_μ are very well known. Numerically one has

$$\delta(1 - \Delta r) \simeq \left[22.3 \left(\frac{\delta M_W}{M_W}\right)^2 + 43.3 \left(\frac{\delta M_Z}{M_Z}\right)^2 \right]^{1/2} \qquad \text{(III.9)}$$

One sees from the above that knowing M_W and M_Z to an accuracy of 1% - which is the situation at the present moment from collider measurements [21] - gives an error $\delta(1 - \Delta r) \simeq 0.08$, which is of the same size as the effect. However, if one could measure both M_W and M_Z to one part per mil, the error in $(1 - \Delta r)$ would be at the percent level, thereby allowing a test of the effect. Indeed, with such an accuracy the error is of the size of what a 1 TeV Higgs would contribute. So with this accuracy one is really looking at the "interesting" part of the radiative mass shift.

At LEP I one will certainly measure the Z^0 mass to a precision of one per mil [22]. Furthermore, by also doing an extremely accurate measurement of the forward - backward asymmetry in $e^+e^- \to \mu^+\mu^-$, it may be possible to test Δr to the percent level [22]. What we will show in the next subsection is that LEP II can determine M_W to 100 MeV and thus provide an alternative check on Δr, at this same level. Because of the fundamental nature of Eq (III.8), such a measurement remains of crucial importance, even if at LEP I one achieves the wanted accuracy.

III.2 Methods for Measuring the W mass

There appear to be at least four independent methods to measure the W mass. They involve:

i) Measuring the threshold dependence of the cross section $e^+e^- \to W^+W^-$

ii) Measuring the end point of the electron spectrum from $W \to e\nu$ decays

iii) Measuring the jet - jet invariant mass from $W \to q\bar{q}$ decays

iv) Measuring the $e\nu$ invariant mass from $W \to e\nu$ decays

Obviously the first method requires an energy scan. However, for the other three cases one can operate at $E_b \simeq 90 - 100$ GeV where the W^+W^- cross section has its maximum. As we will see in the following, the statistical and systematic errors of all four methods [(ii) is a little worse] are all in the range of 100 MeV. Furthermore, a possible overall error in the energy value of LEP also seems to be well in control, with $(\delta E_b)_{LEP} \simeq 10$ MeV [23]. Because the methods are independent, it appears reasonable to expect therefore that a measurement of M_W to $1^0/oo$ will indeed be possible at LEP II.

III.2i) M_W from Threshold Dependence

The total cross section for $e^+e^- \to W^+W^-$ given in Eq (I.1) grows very fast at threshold. This is seen graphically in Fig 24, which shows this behavior for three different W mass values. To a very good approximation near threshold, the complicated expression for the W pair cross section given in Eq (I.1) can be replaced by

$$\sigma_{Thresh.}(e^+e^- \to W^+W^-) \simeq \frac{\pi\alpha^2}{\sin^4\theta_W s}\,\beta \simeq (46\text{pb})\beta \qquad \text{(III.10)}$$

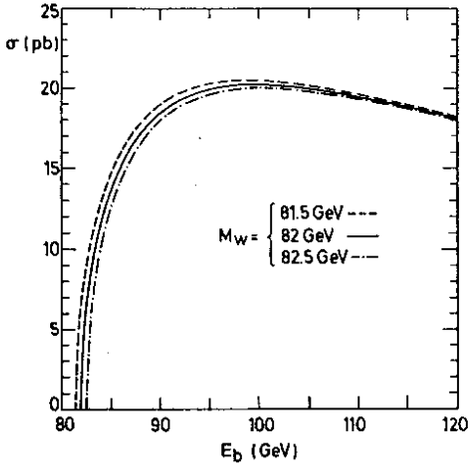

Fig 24: Cross section for $e^+e^- \to W^+W^-$ for three different values of M_W

From the above, or Fig 24, one sees that already 500 MeV above threshold ($\beta \simeq 0.11$) the W^+W^- cross section is close to 5 pb. Obviously with such a fast rise it is incorrect to neglect the effects of the finite width of the W, which is several GeV.

The W width is also affected by radiative corrections. However, these are mostly included by expressing the width in terms of the physical mass of the W. One has [24]

$$\Gamma_W = \frac{G_\mu M_W^3}{6\pi\sqrt{2}} \cdot \frac{(1 + \delta\Gamma)}{B(W\to e\nu)} \qquad \text{(III.11)}$$

where the theoretical correction $\delta\Gamma$ is calculated to be

$$\delta\Gamma \simeq 0.003 \qquad \text{(III.12)}$$

The branching ratio $B(W \to e\nu)$ depends slightly on the value assumed for the top mass. For m_t = 40 GeV, $B(W \to e\nu)$ = 0.089. At any rate, given the dependence of Γ_W on M_W, it is possible to calculate, for a given M_W, the W^+W^- cross section including the effects of finite width. The result of such a calculation, using M_W = 82.5 GeV and Γ_W = 2.80 GeV is shown in Fig 25. Only events where both W masses lie in the interval $M_W \pm \Delta$ are included.

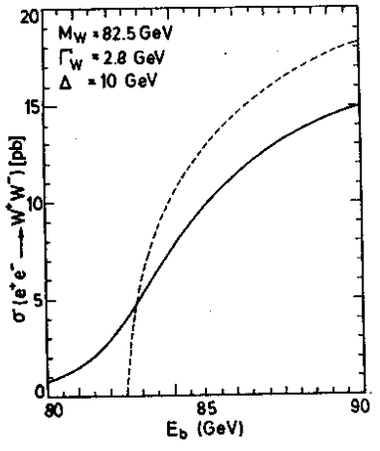

Fig 25: Cross section for $e^+e^- \to W^+W^-$, including effects of the finite W width

One may estimate, very roughly, the expected statistical error on M_W by computing the change in the cross section at 84 GeV as one changes the W mass by one GeV. We find change

$$\delta\sigma = 2.7 \text{ pb} \qquad \text{(III.13)}$$

Thus the precision in the W mass measurement is just

$$\Delta M_W \simeq \frac{1}{2.7} \Delta\sigma \left(\frac{\text{GeV}}{\text{pb}} \right) \qquad \text{(III.14)}$$

where $\Delta\sigma$ is the error on the cross section measurement. For an integrated

luminosity of 100 pb^{-1}, measured at 84 GeV, $\Delta\sigma \simeq 0.25$ pb so that $\Delta M_W \simeq 95$ MeV. Obviously, 100 pb^{-1} is probably an unrealistic estimate for the integrated luminosity that one will collect for any one energy near threshold. However, it is clear already that an error around 100 MeV for M_W is within reach.

One can try to optimize the procedure for extracting a good value of M_W, by studying how best to distribute a realistic amount of running time, as a function of beam energy near the W^+W^- threshold. An attempt in this direction is shown in Fig 25, which leads to a statistical error on M_W of 138 MeV.

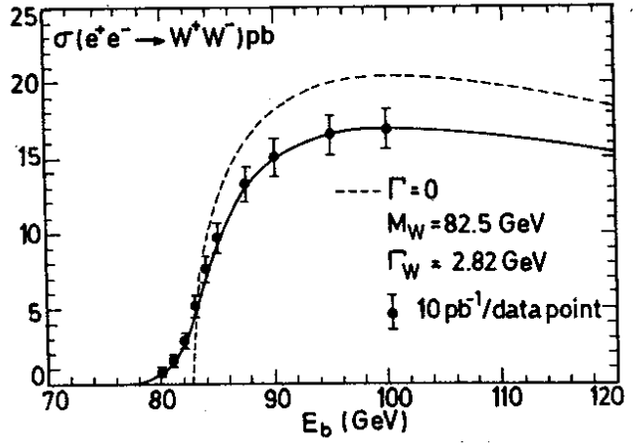

Fig 26: Statistical errors and running time distribution to obtain δM_W = 138 MeV

III.2ii) End point of electron spectrum determination of M_W

Kovalchuk, Rekalo and Stoletnii [25] suggested recently that a good way to measure the W mass in the process $e^+e^- \to W^+W^-$ is by studying the end point of the electron spectrum in $W \to e\nu$ decays. The idea is very simple. Kinematically the electron from W decay, in the W rest system has an energy $\frac{1}{2} M_W$. In the lab system this energy needs to be boosted and it will take its maximum (minimum) values when the electron is emitted in (against) the direction of motion of the W. A simple calculation gives for the electron energy

$$\omega_- \leq E_e \leq \omega_+ \qquad \text{(III.15)}$$

with

$$\omega_\pm = \left(\frac{1\pm\beta}{2}\right) E_b \qquad \text{(III.16)}$$

Clearly measuring $\omega_\pm$ gives β and therefore the W mass.

This simple discussion is, however, changed when one takes into account the fact that the W has a non negligible width. The electron energy spectrum now does not cut off at $\omega_\pm$ but has a tail, as illustrated in Fig 27. The electron spectrum, from $W \to e\nu$, shown in this figure was generated by means of a Monte Carlo programm of Kleiss [7] for the process $e^+e^- \to W^+W^-$, in which finite width effects are included. Clearly, from a statistical point of view the measurement of the spectrum near its upper end (ω_+) is favoured.

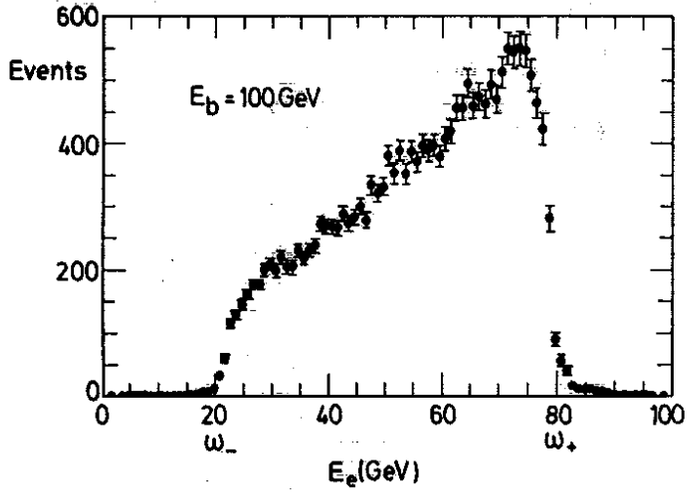

Fig 27: Electron spectrum from $W \to e\nu$ at E_b = 100 GeV

For an integrated luminosity of 500 pb^{-1} one expects roughly 1800 $W \to e\nu$ decays. Of these decays roughly 100 will lie in the last 2 GeV where the spectrum drops sharply. This region of Fig 27 is shown in Fig 28. Hence, applying the same kind of approximate reasoning as before, the statistical error on M_W should be of the order of 200 MeV. For 100 pb^{-1} of integrated luminosity this error climbs to 450 MeV, unless one can include more events

in the analysis than those which enter in the tail. This does not seem likely, as it is really the region near ω_+ which is sensitive to the W mass.

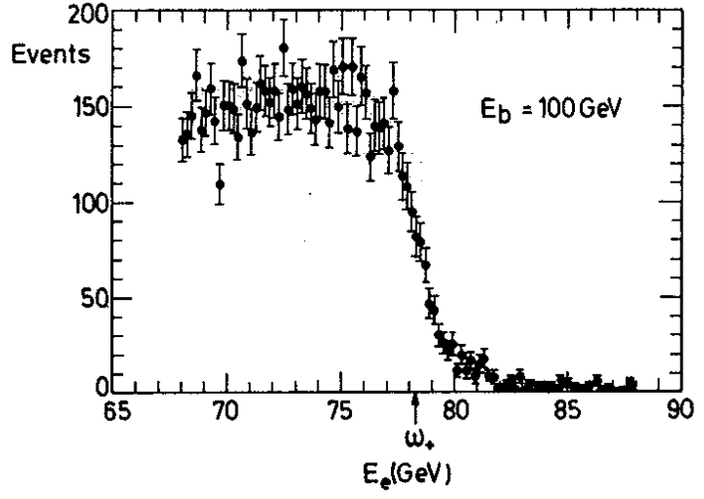

Fig 28: Enlargement of the end point of the electron spectrum from $W \to e\nu$ decays

To the above statistical error one must add a systematic error from the energy calibration of the detector of perhaps 0.2 %. Backgrounds from more complicated decay processes like $W \to \tau\nu$, $\tau \to e\nu\bar{\nu}$ appear to be negligible. Radiative effects, which also affect the electron spectrum, can be mostly corrected for. So the method is nice, but is probably limited by statistical considerations to really serve for a precise determination of M_W.

III.2iii) W mass from di-jet invariant mass

A rather precise determination of the W mass can be obtained by calorimetric methods in decays in which the W decays hadronically. This appears at first sight somewhat surprising because of the expected losses in the calorimeter. However, the trick is that here one is dealing with a constrained system, in which the total hadronic energy is constrained to be equal to the beam energy. A typical $e^+e^- \to W^+W^-$ event in which both W's decay hadronically is shown schematically in Fig 29. Once the W^+W^- axis is reconstructed kinematically, the two jet invariant mass M_{2j} should give directly M_W. However, this will

always be in error because of losses and the energy resolution of the calorimeter. Forcing, however, the energies in the 2 jet system to add up to E_b ($E_{2j} = E_b$)constrains the system considerably.

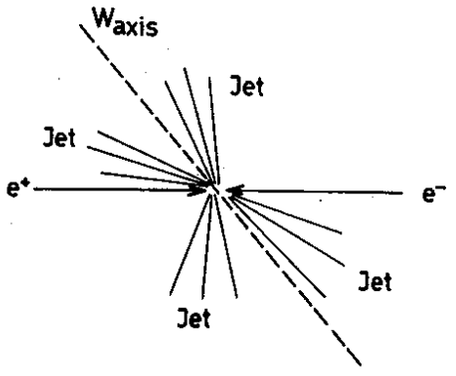

Fig 29: $e^+e^- \rightarrow W^+W^- \rightarrow 4$ jets

P. Roudeau describes in Appendix C a Monte Carlo analysis of this problem for DELPHI. Here we shall just give the essential results of his analysis. In the Monte Carlo simulation only 4 jet W^+W^- events are considered, although in principle one could also study 2 jets lν events. Events are generated for E_b = 100 GeV, assuming M_W = 83.2 GeV and Γ_W = 0. If one selects W events by picking, out of the 4 jets, 2 jet combinations which have M_{2j} near E_b, one finds the jet - jet mass distribution shown in Fig 30. The output mass obtained for the W from this procedure is M_W = 81.5 ± 0.33 GeV and Γ_W = 4.7 ± 0.11 GeV. That is, there is about a 2 GeV "loss" from the input mass value. This is not surprising since no constraint was imposed on the 2 jet events. Demanding that $E_{2j} = E_b$, on the other hand, makes a tremendous difference. The result of the analysis is shown in Fig 31. First of all the width of the peak is considerably narrowed (Γ_W = 1.769 ± 0.046 GeV) and the peak is shifted to M_W = 83.105 ± 0.012 GeV.

The above results are very encouraging, although more realistically one should include width effects. Clearly the statistical error on M_W is totally negligible, but that perhaps is to be expected. The systematic error,

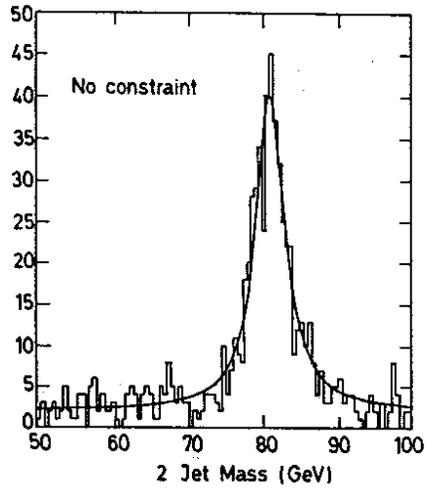

Fig 30: Reconstructed 2 jet mass with no constraint on E_{2j}

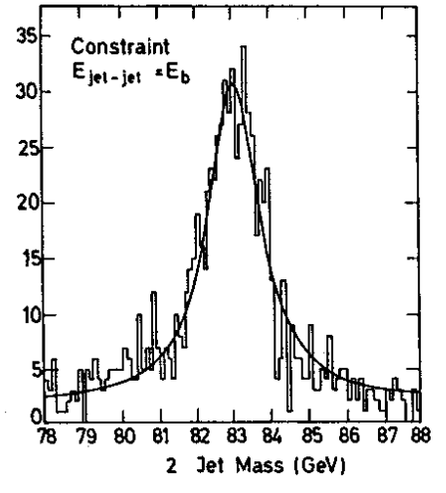

Fig 31: Reconstructed 2 jet mass with the constraint $E_{2j} = E_b$

if the above energy shift can be considered an indication, also appears to be very small. The constraint $E_{2j} = E_b$ effectively renormalizes the losses of the detector, making them very much smaller. It is the constrained nature of the process that makes an accurate W mass measurement by calorimetric methods possible. This would never be possible in hadronic production of the

W bosons, even if one could magically eliminate other 2 jet background. No constraints exist in hadronic colliders to recalibrate the calorimeter.

Obviously the above Monte Carlo discussion may underestimate the actual systematic error in the analysis. One may perhaps "test" this procedure at LEP I operating at the Z^0. It would be very interesting to see the accuracy with which the Z^0 mass can be determined from hadronic Z^0 decays, once the constraint $E_{2j} = 2E_b$ is imposed. A kinematically perhaps more akin process, where this test could also be done, would be $e^+e^- \to Z^0\gamma$, with the Z^0 decaying into two jets. Again, it would be useful to know the accuracy achievable for M_{Z^0}, once the constraint $E_{2j} = 2\,E_b - E_\gamma$ is imposed.

III.2iv) W Mass from $e\nu$ invariant mass

The final way we have considered for obtaining a value for M_W is by using the decay $W \to e\nu$ and trying to compute the $e\nu$ invariant mass, in a manner analogous to what was just described. Consider for example the 2 jet $e\nu$ decay shown schematically in Fig 32. The kinematics is totally determined once the W axis is fixed and the electron energy and scattering angle are measured. One has

$$M^2_W = 2\,E_e\,E_\nu(1 - \cos\theta_{e\nu}) \qquad \text{(III.17)}$$

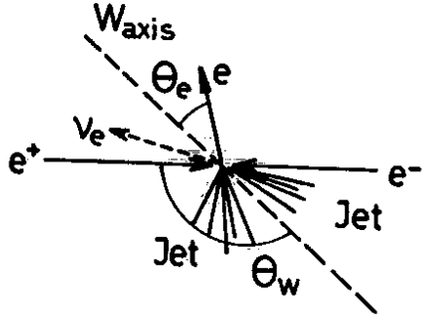

Fig 32: $e^+e^- \to W^+W^- \to$ 2 jets $e\nu$

with the neutrino energy being given by $E_\nu = E_b - E_e$. The angle $\theta_{e\nu}$ between the electron and the neutrino is known from a measurement of θ_W and θ_e, since the neutrino momentum transverse to the W direction must balance that of the

electron direction. In contrast to what is measured at hadron colliders, which is $M^T_{e\nu}$, the transverse $e\nu$ invariant mass, at LEP II one really can measure $M_{e\nu} = M_W$.

Fig 33 shows the distribution in $M_{e\nu}$ obtained by a Monte Carlo analysis of 2400 W^+W^- events at E_b = 100 GeV [This analysis is described in more detail in Appendix C]. The value obtained for M_W is M_W = 83.120 ± 0.055 GeV, which has a very small statistical error. Since the starting value for M_W was 83.20 GeV, one observes again a small systematic underestimate of the final mass. To this systematic error one should add other errors coming from the electron energy calibration and angular measurement, so that probably the total systematic error would be over 100 MeV. Nevertheless, also this technique looks rather promising.

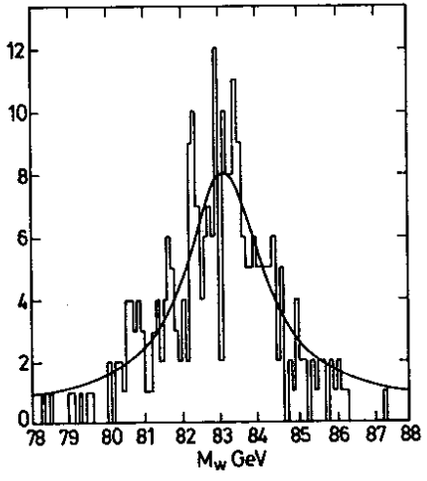

Fig 33: Kinematically reconstructed $e\nu$ mass

III.3 W decays

In the standard model, the W couples universally to fermion pairs. For the leptons, universality means precisely equal coupling of the W to the $\bar{e}\nu_e$, $\bar{\mu}\nu_\mu$ and $\bar{\tau}\nu_\tau$ pairs. For the quarks, because the mass eigenstates are not the weak interaction eigenstates, the W can have couplings which are not generation diagonal. However, the coupling matrix is unitary, so that universality, in this broader sense, obtains.

To be specific, the charged weak bosons couple to the charged currents $J_\pm^\mu$ as

$$L_{int} = \frac{e}{2\sqrt{2}\sin\theta_W} \left[J_+^\mu W_{-\mu} + J_-^\mu W_{+\mu} \right] \qquad \text{(III.18)}$$

In terms of the quark and lepton fields, these currents read, for the case of three generations:

$$J_+^\mu = (\bar{\nu}_e\ \bar{\nu}_\mu\ \bar{\nu}_\tau)\gamma^\mu(1-\gamma_5)\ 1 \begin{pmatrix} e \\ \mu \\ \tau \end{pmatrix} + (\bar{u}\ \bar{c}\ \bar{t})\gamma^\mu(1-\gamma_5)\ V_{KM} \begin{pmatrix} d \\ s \\ b \end{pmatrix}$$

$$J_-^\mu = (J_+^\mu)^\dagger \qquad \text{(III.19)}$$

The Kobayashi - Maskawa matrix [26] V_{KM} is unitary

$$V_{KM}^\dagger V_{KM} = 1 \qquad \text{(III.20)}$$

so that the magnitude of the overall coupling of the W bosons to leptons and quarks (of each colour) is the same.

The partial decay rates of the W into quark pairs measure, therefore, the elements of the Kobayashi - Maskawa matrix directly. The total rate will be independent of V_{KM}, provided one neglects the effect of the quark masses. This is fine for all quarks, except the top. Keeping only the top mass just changes the overall rate by a calculable phase space factor. One has [27]

$$\Gamma(W\to all) = \Gamma(W\to\bar{e}\nu_e) \left\{ 3 + 3\left[2 + \left(1 + \frac{m_t^2}{2M_W^2} \right) \left(1 - \frac{m_t^2}{M_W^2} \right)^2 \right] \left(1 + \frac{\alpha_s}{\pi} \right) \right\} \qquad \text{(III.21)}$$

The first factor in the curly bracket is the contribution of the leptonic channels, while the second is due to the hadronic channels. The factor of $(1+\frac{\alpha_s}{\pi}) \approx 1.04$ is the leading QCD correction to the result. Note that for $m_t = 40$ GeV, the phase space reduction in the t quark decay mode is already substantial (to ~ 65 % of the light quark value).

The branching fractions for W decays are, therefore

$$B(W\to\bar{l}\nu_l) = \left\{ 3 + 3\left[2 + \left(1 + \frac{m_t^2}{2M_W^2} \right) \left(1 - \frac{m_t^2}{M_W^2} \right)^2 \right] \left(1 + \frac{\alpha_s}{\pi} \right) \right\}^{-1} \approx 0.089 \qquad \text{(III.22a)}$$

$$B(W\to\bar{q}q') = 3|V_{qq'}|^2 \left(1 + \frac{\alpha_s}{\pi} \right) \left\{ 3 + 3\left[2 + \left(1 + \frac{m_t^2}{2M_W^2} \right) \left(1 - \frac{m_t^2}{M_W^2} \right)^2 \right] \left(1 + \frac{\alpha_s}{\pi} \right) \right\}^{-1} \approx 0.277\ |V_{qq'}|^2 \qquad (q,q'\neq t) \qquad \text{(III.22b)}$$

$$B(W\to\bar{t}q) = \frac{3|V_{tq}|^2 \left(1 + \frac{m_t^2}{2M_W^2} \right) \left(1 - \frac{m_t^2}{M_W^2} \right)^2 \left(1 + \frac{\alpha_s}{\pi} \right)}{\left\{ 3 + 3\left[2 + \left(1 + \frac{m_t^2}{2M_W^2} \right) \left(1 - \frac{m_t^2}{M_W^2} \right)^2 \right] \left(1 + \frac{\alpha_s}{\pi} \right) \right\}} \approx 0.180\ |V_{tq}|^2 \qquad \text{(III.22c)}$$

The numerical values given in E_{qs} (III.22) correspond to the specific choice $m_t = 40$ GeV, which we shall use for illustrative purposes.

The Kobayashi - Maskawa matrix V_{KM} is quite well determined, if one assumes universality (i.e. $V\,V = 1$). Without assuming universality obviously the en-

tries involving the t quark are still undetermined and other entries have large errors. LEP II, by measuring directly W decays into $\bar{t}q$, can check universality. In fact, if the top quark is not in the mass range indicated by the UA1 collaboration [28], it could very well be that W decays at LEP II will be of fundamental importance for determining properties of the top. Furthermore, provided that flavor identification of jets is possible, LEP II can provide a better determination of other elements of V_{KM}. We give in Table I, taken from the review of Kleinknecht [29], the value of the elements of V_{KM} which are directly determined experimentally

Table I: Experimental values of $|V_{KM}|$, from Ref [29]

	d	s	b
u	0.9723 ± 0.0014	0.231 ± 0.003	< 0.004
c	0.24 ± 0.03	0.88 ± 0.10	0.045 ± 0.006
t	?	?	?

To estimate the rate of events expected at LEP II we shall make use of the following values for V_{KM} (Table II). These values are also taken from Ref [29], where direct data has been supplemented by the unitarity condition (III.20).

Table II Plausible values for $|V_{KM}|$ from Ref [29]

	d	s	b
u	0.973	0.231	0.002
c	0.231	0.972	0.045
t	0.010	0.045	0.999

Lep II, as has been repeatedly emphasized, will have a clean sample of W events. With 500 pb^{-1} integrated luminosity we expect, at E_b = 100 GeV, nearly 20000 W decays. Of these approximately 75 % will be hadronic decays. Even assuming only a 50 % detection efficiency, one would be left with a very clean sample of about 7500 $W \to \bar{q}q$ decays. Using Table II and the branching fractions given in Eqs.(III.22b) and (III.22c) (assuming m_t = 40 GeV) one would expect the event distribution shown in Table III.

Table III: Event distribution for 7500 $W \to \bar{q}q$ decays

$\bar{u}d + \bar{d}u$ 2670	$\bar{u}s + \bar{s}u$ 150	$\bar{u}b + \bar{b}u$ 0	Σ_u 2820
$\bar{c}d + \bar{d}c$ 150	$\bar{c}s + \bar{s}c$ 2664	$\bar{c}b + \bar{b}c$ 6	Σ_c 2820
$\bar{t}d + \bar{d}t$ 0	$\bar{t}s + \bar{s}t$ 4	$\bar{t}b + \bar{b}t$ 1856	Σ_t 1860
Σ_d 2820	Σ_s 2818	Σ_b 1862	Σ 7500

If flavor identification of the jets were perfect, it is easy to convince oneself that the statistical accuracy of the above measurements would imply an error of approximately ± 0.010 for each element of V_{KM}. Such an error is certainly in a very interesting range for V_{cd} and V_{cs}, but flavor tagging here is far from perfect. For V_{tb}, where flavor tagging should be quite good, one sees that there is a serious possibility of testing universality at the percent level at LEP II. A detailed analysis of the different channels of W decay and the separation of the different flavours in the light of a specific detector is under study with Monte Carlo methods [30]. Here some preliminary main features of the events are presented. They indicate that the possibility to separate $W \to t\bar{b}$ from $W \to q\bar{q}$ (light) seems extremely encouraging. In Fig 34 a typical event involving $t\bar{b}$ is shown, which is characterized by a multijet topology with many soft particles. For the Monte Carlo generation, a top mass of 40 GeV and a center of mass energy of 170 GeV were assumed.

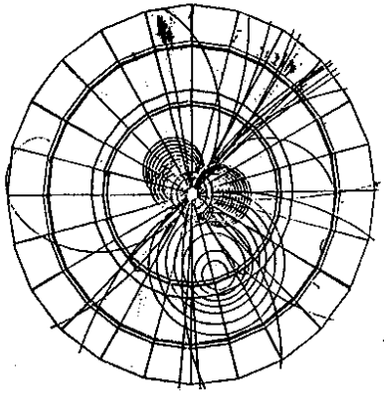

Fig 34: Typical event showing $W^+ \to t\bar{b}$ and $W^- \to e\bar{\nu}$ decay patterns

Fig 35a shows the thrust distribution of events of the kind $W \to t\bar{q}$ compared to $W \to u\bar{q} + c\bar{q}$, while Fig 35b shows the number of jets in these decays.

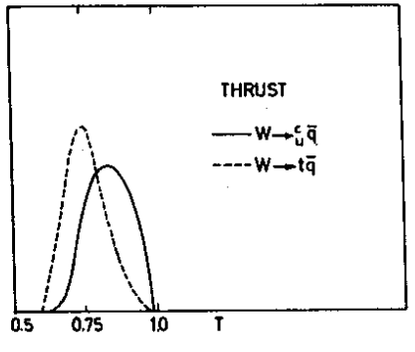

Fig 35a: Thrust distributions for $W \to t\bar{q}$ and $W \to u\bar{q} + c\bar{q}$

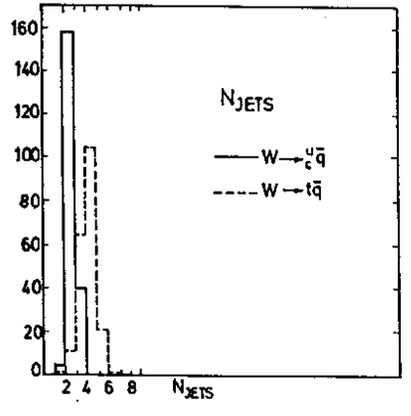

b: Number of jets for $W \to t\bar{q}$ and $W \to u\bar{q} + c\bar{q}$

In principle the study of $|V_{KM}|$ is further simplified if one of the W decay leptonically giving an energetic lepton and a neutrino, so that the final state contains only two hadronic jets. The leptonic decay reduces, of course, the total number of W's for the study but it provides a strong experimental signature and it avoids jet misidentification.

IV $e^+e^- \to Z^0Z^0$ AND HIGGS SEARCHES AT HIGH ENERGY

The reaction $e^+e^- \to Z^0Z^0$, in contrast to W pair production, has little intrinsic physics interest. This is because:

1)All relevant properties of the Z^0 should be already very well known by the time LEP II comes into operation.

2)The reaction itself involves no new vertices in the standard model, besides the $e^+e^-Z^0$ vertex, as is seen from Fig 36.

3)The cross section for Z^0 pair production is rather small.

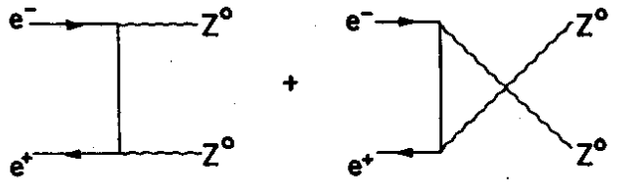

Fig 36: The process $e^+e^- \to Z^0Z^0$ in lowest order

This last point can be gleaned from the formula for the total cross section [31]:

$$\sigma_{TOT}(e^+e^- \to Z^0Z^0) = \frac{\pi\alpha^2 \left[1 + 6(1 - 4\sin^2\theta_W)^2 + (1 - 4\sin^2\theta_W)^4\right]}{64\sin^4\theta_W\cos^4\theta_W s}$$

$$\cdot \left\{ \frac{4M_Z^4 + s^2}{s(s - 2M_Z^2)} \ln\frac{(1 + \beta_Z)}{(1 - \beta_Z)} - \beta_Z \right\} \qquad \text{(IV.1)}$$

where $\beta_Z = (1 - 4M_Z^2/s)^{1/2}$. Near threshold, this formula reduces to

$$\sigma_{Thresh}(e^+e^- \to Z^0Z^0) \simeq \frac{\pi\alpha^2[1 + 6(1- 4\sin^2\theta_W)^2 + (1- 4\sin^2\theta_W)^4]\,\beta_Z}{16\sin^4\theta_W\cos^4\theta_W\, s}$$

$$\simeq (5\text{ pb})\,\beta_Z \qquad \text{(IV.2)}$$

Comparison with Eq (III.10) shows that, at equivalent β values, the Z^0Z^0 cross section (essentially because $\sin^2\theta_W \simeq 1/4$) is almost an order of magnitude smaller than the W^+W^- cross section.

Unfortunately, the $e^+e^- \to Z^0Z^0$ reaction provides a serious background for high mass Higgs searches. A detailed treatment of methods for finding Higgs bosons at LEP is contained in [2]. Here we only focus on the mass range $2m_t \lesssim m_H \lesssim 2M_W$, for which hadronic production experiments are largely ineffective [32] and for which LEP II may be quite useful.

The dominant production process for Higgs bosons in the LEP II energy range is in association with a Z^0 boson, as shown in Fig 37. The total cross section for this process is given by [33]

$$\sigma_{TOT}(e^+e^- \to HZ^0) = \frac{\pi\alpha^2 P[3M_Z^2 + P^2]\,[1 + (1 - 4\sin^2\theta_W)^2]}{24\sin^4\theta_W\cos^4\theta_W/s\,(s - M_Z^2)^2} \qquad \text{(IV.3)}$$

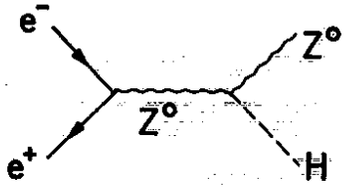

Fig 37: Dominant diagram for Higgs production at LEP II

where P is the 3-momentum of the Z^0 :

$$P = \frac{1}{2}\left[s - 2M_Z^2 - 2m_H^2 + \frac{1}{s}\left(M_Z^2 - m_H^2 \right)^2 \right]^{1/2} \qquad \text{(IV.4)}$$

This cross section is plotted in Fig 38, for various values of M_H. As can be seen, it is significant (i.e. $\sigma_{peak} \gtrsim 0.1$ pb) even for $M_H \simeq 2M_W$.

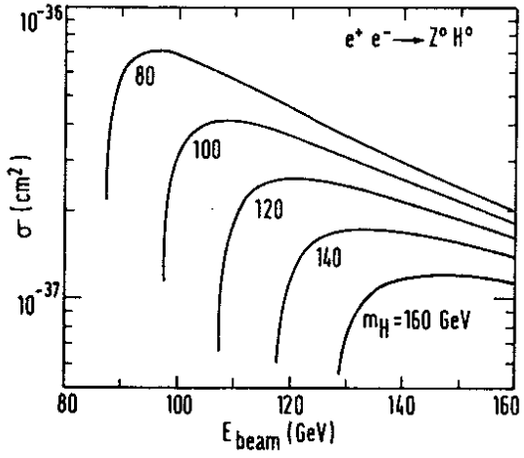

Fig 38: Cross section for the process $e^+e^- \to Z^0H$, for various values of M_H, as a function of beam energy.

Of course with $E_b^{Max} \simeq 100$ GeV, available at LEP II, only $M_H \lesssim 100$ GeV will be accessible. Since LEP I should be sensitive to Higgs bosons with $M_H \lesssim$ 70 GeV, if toponium exists near M_Z [34], LEP II experiments should aim to cover the region above this range. However, it is precisely in this region where the process $e^+e^- \to Z^0Z^0$ will give a nontrivial background for the Higgs search via $e^+e^- \to Z^0H$.

Assuming an integrated luminosity of 500 pb^{-1} / year one will collect approximately 850 Z^0Z^0 events at $E_b = 100$ GeV. For the Higgs search, one is interested in tagging the Z^0 through its leptonic decay and reconstructing the Higgs as a peak in the recoil mass spectrum. The Z^0Z^0 events provide a background of around 75 events of the type e^+e^- 2 jets or $\mu^+\mu^-$ 2 jets, which have the same signature as that for the Higgs search. The signals for m_H = 80, 90 and 100 GeV are, respectively, 20, 15 and 9 events of this type. Clearly to identify this signal within the Z^0Z^0 background will require good recoil mass resolution, to be able to distinguish a Z^0 peak at mass M_Z0 from an H peak at mass m_H.

Experimentally one taggs on a lepton pair from $Z^0 \to l\bar{l}$ (e^+e^- or $\mu^+\mu^-$), so that the recoil mass is

$$M^2_{\text{recoil}} = (\sqrt{s} - E_l - E_{\bar{l}})^2 - (\vec{p}_l + \vec{p}_{\bar{l}})^2 \qquad \text{(IV.5)}$$

$$= s - 2\sqrt{s}(E_l + E_{\bar{l}}) + M^2_{l\bar{l}}$$

where $M_{l\bar{l}}$ denotes the invariant mass of the tagged $l\bar{l}$ system. The recoil mass resolution is then determined by the energy and angular resolution of the lepton momenta via

$$2M_{\text{recoil}}\,\Delta M_{\text{recoil}} = -2\sqrt{s}(\Delta E_l + \Delta E_{\bar{l}}) + 2M_{l\bar{l}}\,\Delta M_{l\bar{l}} \qquad \text{(IV.6)}$$

Since $2M_{\text{recoil}} \simeq 2M_{l\bar{l}} \simeq \sqrt{s}$ in the present case, we estimate the resolution as

$$\Delta M_{\text{recoil}} \simeq [(2\Delta E_l)^2 + (2\Delta E_{\bar{l}})^2 + (\Delta M_{l\bar{l}})^2]^{1/2} \qquad \text{(IV.7)}$$

In the case of the electron shower energy, if $\Delta E_e/E_e \sim 1\%$ at 50 GeV, we expect $\Delta E_{e^-} \simeq \Delta E_{e^+} \simeq 0.5$ GeV and the e^+e^- invariant mass can be measured with an accuracy of 1 GeV. Hence an accuracy of approximately 2 GeV on the recoil mass seems within reach. Provided $|M_H - M_{Z^0}| \gtrsim 5$ GeV, one should be able to separate the Z^0 and H bumps in the recoil mass spectrum. Having found an extra bump in this spectrum, it should not be too difficult to identify the Higgs boson by studying the recoil jet system carefully, since this system should consist mainly of $b\bar{b}$ or $t\bar{t}$ pairs.

If the Z^0 is identified by its $\mu^+\mu^-$ -mode, one probably cannot expect enough mass resolution, with the notable exception of the L3 experiment, to proceed in the above way. In this case, or if $|M_H - M_{Z^0}| \lesssim 5$ GeV, one should look for an excess of events of a $b\bar{b}$ or $t\bar{t}$ origin. Although one may expect that the $t\bar{t}$ events can be identified with a reasonable probability, it probably will be impossible to reconstruct the invariant mass of the system from jet studies, to a good enough accuracy. However, once such an excess of $t\bar{t}$ or $b\bar{b}$ events is observed associated with $Z^0 \to \bar{l}l$ decays, it should be confirmed in other channels, particularly those involving associated $Z^0 \to \bar{\nu}\nu$ decays.

For Higgs bosons with $M_H \lesssim 85$ GeV, running LEP II at energies below the Z^0Z^0 threshold would be quite advantageous, since one can then forget entirely

about this background. To give an example, running at $E_b = 90$ GeV one still expects in one year nearly 20 events of the type e^+e^- 2 jets or $\mu^+\mu^-$ 2 jets for a Higgs mass of 80 GeV. Since there is here no Z^0Z^0 background, these events are clean. In addition, equally clean and spectacular are events in which the Z^0 decays into neutrino pairs. For $m_H = 80$ GeV one expects 60 events of the type: missing energy in one hemisphere plus two jets in the other hemisphere. If indeed $m_H > 2m_t$, then the hadronic jets in the Higgs decay will be essentially only t-quark jets, which should help the identification further. If $H \to b\bar{b}$ is the main decay mode, one may be able to use the angular distribution of the dijet system to infer that a spin 0 object was produced.

V. COMPOSITENESS TESTS AT LEP II

It has been widely speculated that quarks and leptons may not be elementary objects after all, but have themselves substructure [35]. If quarks and leptons are composite one expects three distinct classes of phenomena to occur:

i) The interactions among quarks and leptons at sufficiently high energy will begin to show departures from the point-like behaviour, characteristic of the standard model with elementary fermions.

ii) Excited states of both leptons and quarks should begin to be observed.

iii) Possible exotic states, like leptons with color or quarks which are not SU(3) triplets, may also appear.

Because all of these phenomena can be well studied in high energy e^+e^- collisions, LEP II offers an invaluable opportunity for probing further into the nature of quarks and leptons.

V.1: Contact interactions and compositeness bounds at LEP II

If electrons were not pointlike objects, their intrinsic size would be characterized by a scale Λ_{ee}, such that $\langle r \rangle \sim \frac{1}{\Lambda_{ee}}$. Of course, this way of defining an electron radius is not very precise. One should really specify more closely with what reaction one is probing the electrons. The scale of compositeness of an electron probed electromagnetically may well be slightly different than that emerging from e^+e^- collisions.

It has become conventional to define the scale of compositeness Λ_{ee} , by considering the effects that substructure would have in Bhabha scattering [36]. If electrons have substructure, one expects residual interactions to exist among them, above and beyond those of the standard model. One can characterize these interactions by introducing contact terms, scaled by powers of Λ_{ee} , involving operators containing 4 electrons, 6 electrons, etc. This is indicated schematically in Fig 39. For energies much below the scale Λ_{ee} only the contact interactions involving four electron fields are relevant, all other terms being down by powers of $(\sqrt{s} / \Lambda_{ee})$.

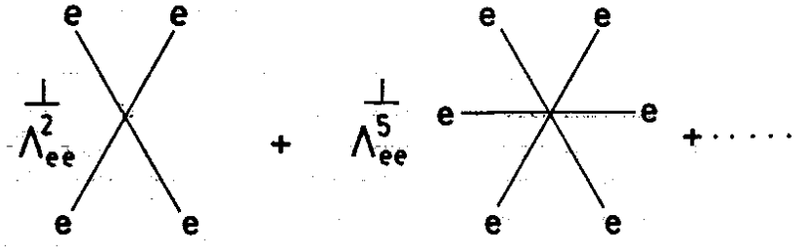

Fig 39: Contact interactions which arise if the electron is composite

Eichten, Lane and Peskin [36] have parametrized these interactions in a standard form, involving operators which do not cause helicity flip. (Helicity flip operators are presumed to be suppressed by powers of m_e / Λ_{ee} , and thus are negligible). The residual electron interactions read

$$L_{ee}^{eff} = \frac{g^2}{2\Lambda_{ee}^2} \sum_{i,j = L,R} \eta_{ij} (\bar{e}_i \gamma_\mu e_i) (\bar{e}_j \gamma^\mu e_j) \qquad (V.1)$$

Here e_L, e_R are the usual helicity projections

$$e_L = \frac{1}{2} (1-\gamma_5)e \; ; \qquad e_R = \frac{1}{2} (1+\gamma_5)e \qquad (V.2)$$

The coupling constant g^2 , since the residual interactions must arise from some underlying strong coupling theory, is large. Conventionally [36], one assumes that

$$g^2 / 4\pi = 1 \qquad (V.3)$$

which serves to define Λ_{ee} . Finally the parameters η_{ij} are variously assumed to be ±1 or 0, so that the residual interactions take specific helicity forms (e.g. $\eta_{LL} = \eta_{RR} = \eta_{LR} = \eta_{RL}$ gives purely vectorial residual interactions, etc).

In addition to the residual interactions among electrons given in (V.1), if electrons and muons (or electrons and quarks) have the same constituents one expects also contact terms involving electrons and muons (or electrons and quarks). These terms will invove inverse powers of a new scale $\Lambda_{e\mu}$ (Λ_{eq}), which could be the same as Λ_{ee} , but need not necessarily be so. We detail such a term for the e-μ case; the e-q term is written analogously:

$$L_{e\mu}^{eff} = \frac{g^2}{\Lambda_{e\mu}^2} \sum_{i,j = L,R} \eta_{ij} (\bar{e}_i \gamma_\alpha e_i) (\bar{\mu}_j \gamma^\alpha \mu_j) \qquad (V.4)$$

Here g^2 again is, conventionally, taken to be equal to 4π (cf Eq V.3) and $\eta_{ij} = \pm 1$ or 0.

There exist already bounds on the scales Λ_{ee} and $\Lambda_{e\mu}$ coming from experiments at PEP and PETRA. Typically one finds [37]:

$$\Lambda_{ee} \; , \; \Lambda_{e\mu} \gtrsim \text{(1-4) TeV} \qquad (V.5)$$

where the precise values one obtains depend in detail on which particular helicitiy combination for the residual interactions one has assumed. We have examined, analogously, what limits can LEP II, running at E_b = 100 GeV, set on Λ_{ee} and $\Lambda_{e\mu}$, for a given integrated luminosity. The result, broadly speaking, is that LEP II can push the limits on the electron's compositemess scale above 10 TeV.

This contention is illustrated in more detail in Figs 40 and 41, where we plot, as a function of the integrated luminosity collected, the expected 95 % confidence limits on Λ_{ee} and $\Lambda_{e\mu}$, for a variety of possible helicity configurations of L^{eff} . It is clear that, with 500 pb^{-1}, one pushes these limits above 10 TeV, almost irrespective of the detailed helicity structure of L^{eff} .

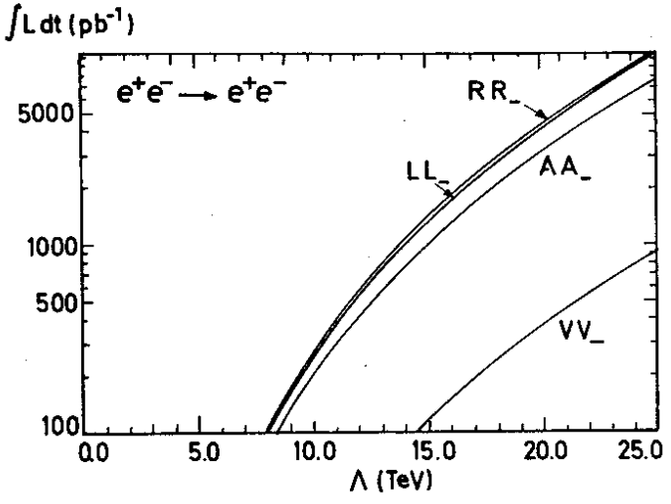

Fig 40a: Limits expected on Λ_{ee} for different helicity configurations which add negatively to the standard model contribution ($\eta_{ij} = -1$)

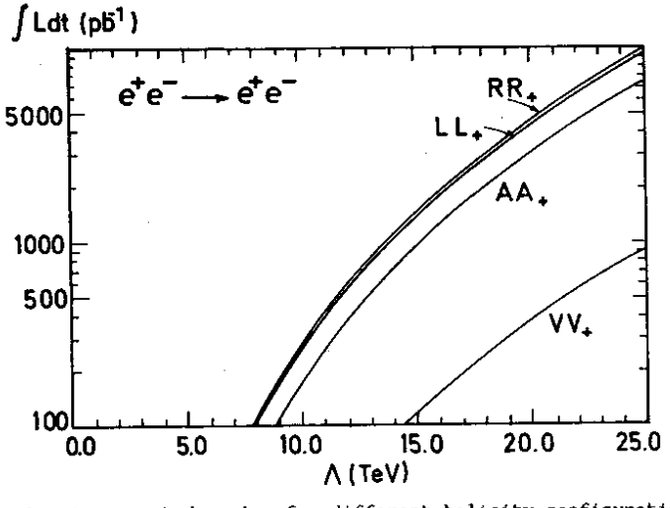

Fig 40b: Limits expected on Λ_{ee} for different helicity configurations which add to the standard model contributions ($\eta_{ij} = +1$)

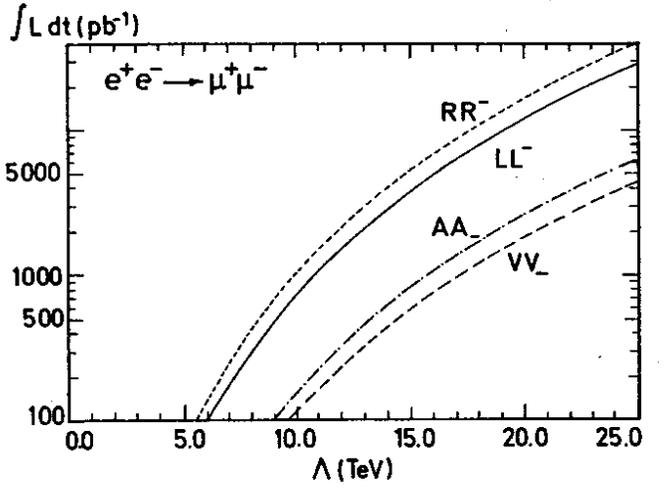

Fig 41a: Limits expected on $\Lambda_{e\mu}$ for different helicity configurations which add negatively to the standard model contributions ($\eta_{ij} = -1$)

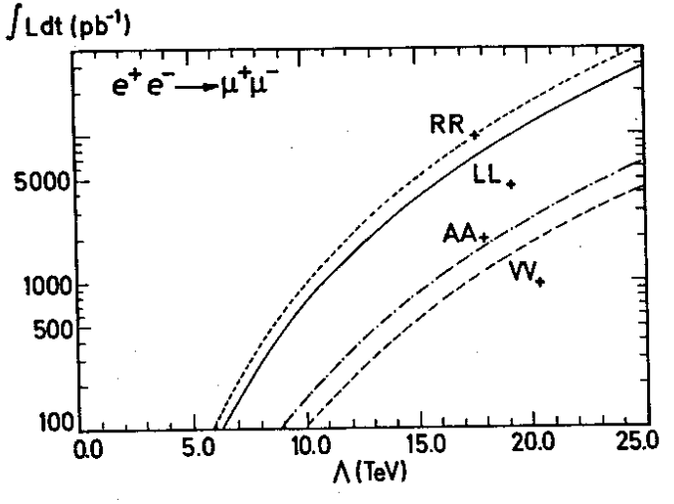

Fig 41b: Limits expected on $\Lambda_{e\mu}$ for different helicity configurations which add to the standard model contribution ($\eta_{ij} = +1$)

This is illustrated in another way in Figs 42 and 43, by plotting the statistical errors expected in the data, compared to the approximate maximum allowed deviations due to compositeness.

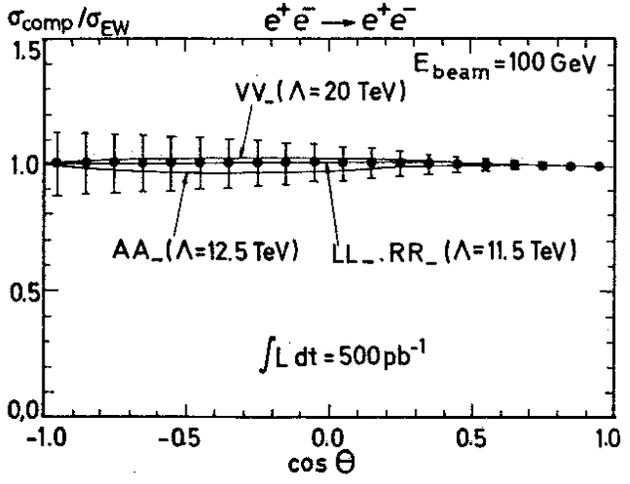

Fig 42: Statistical errors for the process $e^+e^- \to e^+e^-$, for 500 pb^{-1} of data, compared to various deviations due to compositeness.

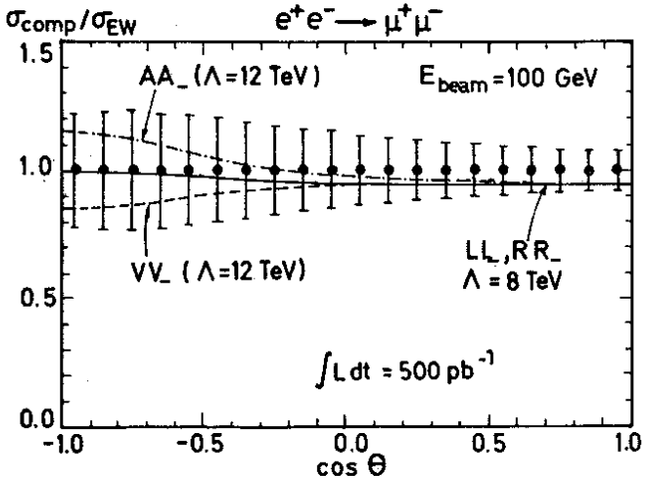

Fig 43: Statistical errors for the process $e^+e^- \to \mu^+\mu^-$, for 500 pb^{-1} of data, compared to various deviations due to compositeness

If indeed deviations from the predictions of the standard model are observed at LEP II, indicating the existence of yet another layer of matter, then one expects <u>asymptotically</u> that the e^+e^- cross section becomes a constant (up to logarithmic factors).

$$\sigma^{\text{Asym.}}_{e^+e^-} \simeq \frac{1}{\Lambda^2_{ee}} \qquad (V.6)$$

This value, for $\Lambda_{ee} \sim 10$ TeV, is of the same order of magnitude as the e^+e^- cross section at LEP II energies. Thus, if one observes sighals of compositeness at LEP II, one can presume that the e^+e^- cross section above these energies will certainly cease to fall with energy (and may indeed rise with energy!) This conclusion does not mean, however, that substructure leads necessarily to larger cross sections in the LEP II energy range. Depending on the precise helicity structure, the contact terms in Eqs (V.1) and (V.4) can lead to either positive or negative interference with the standard model predictions.

We illustrate the above remarks by considering specifically the example of $e^+e^- \to \mu^+\mu^-$ in the case $\Lambda_{e\mu} = 4$ TeV, which is a value of $\Lambda_{e\mu}$ not excluded by PEP-PETRA data. As shown in Figs. 44 depending on whether the parameters in $L^{\text{eff}}_{e\mu}$ are positive or negative, one gets total cross sections for the process $e^+e^- \to \mu^+\mu^-$ in the LEP II energy range which are, respectively, bigger than or smaller than those predicted by the standard model.

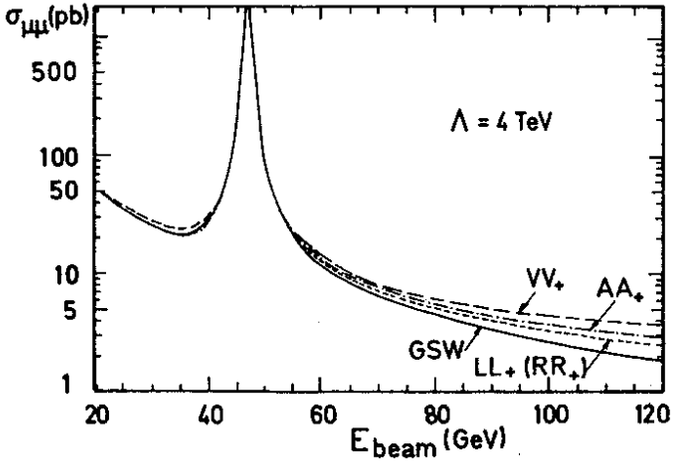

Fig 44a: Positive departures from the standard model values for the process $e^+e^- \to \mu^+\mu^-$, due to compositeness

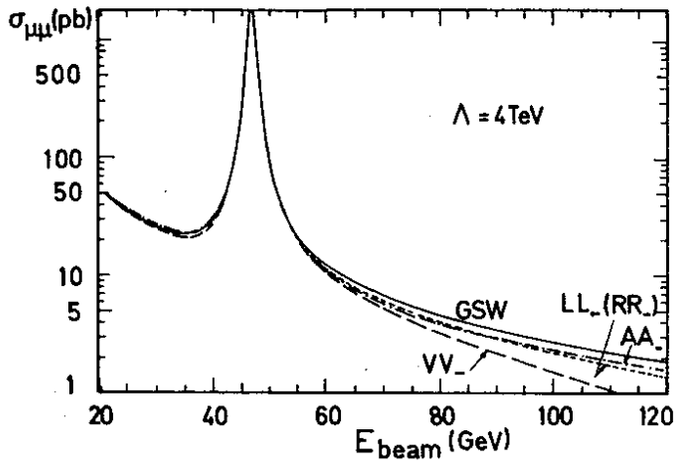

Fig 44b: Negative dapartures from the standard model values for the process $e^+e^- \to \mu^+\mu^-$, due to compositeness

For certain particularly favorable helicity combinations (VV,AA), for $\Lambda_{\mu e}$ = 4 TeV, one gets also sizable changes in the magnitude of the forward backward asymmetry in $e^+e^- \to \mu^+\mu^-$, as illustrated in Figs 45. Similar discrepancies can occur also if there existed heavier Z^0 bosons, a common prediction of superstring theories [38]. For $M_{Z^{0'}} >> M_{Z^0}$, the contribution of these bosons leads to analogous effective interactions as compositeness.

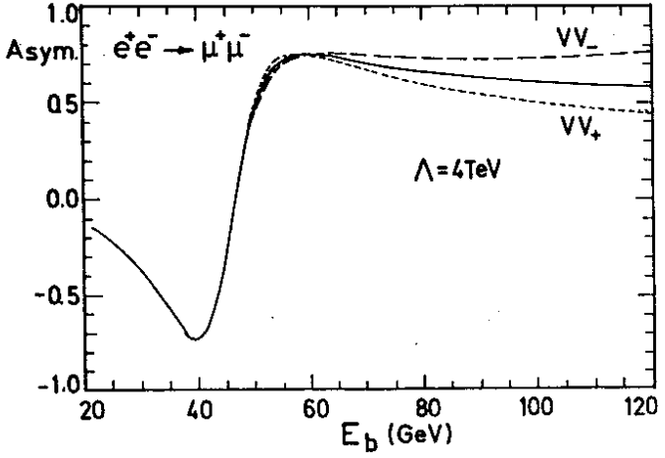

Fig 45a: Departure from the standard model for the $e^+e^- \to \mu^+\mu^-$ asymmetry due to a VV contact interaction

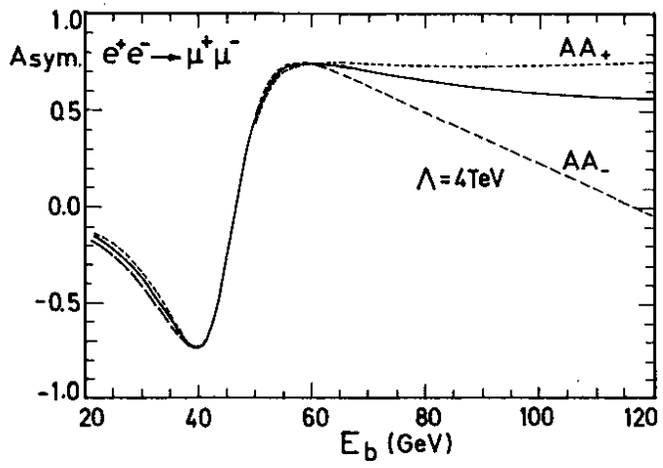

Fig 45b: Departure from the standard model for the $e^+e^- \to \mu^+\mu^-$ asymmetry due to an AA contact interaction

Of course $\Lambda_{\mu e}$ (and Λ_{ee}) may be bigger than 4 TeV and so the above effects may be less pronounced - or not exist at all. We conclude, nevertheless, that LEP II allows, through a careful study of the reactions $e^+e^- \to e^+e^-$ and $e^+e^- \to \mu^+\mu^-$, to probe for substructure of the electron to distances of the order of $\langle r \rangle \sim 10^{-18}$ cm ($\Lambda \sim 10$ TeV).

V2. Excited leptons

If the compositeness scale is really very large ($\Lambda \gtrsim 10$ TeV), one does not expect to have light excited leptons. Roughly speaking, the mass gap between an excited lepton and an ordinary lepton should be of the order of the compositeness scale: $m_l^* - m_l \sim \Lambda_{ll}$. If the compositeness scale is low - of the order of a few TeV - one may not be totally surprised to find an excited lepton in the 100 GeV range. Thus a search for these objects at LEP II is certainly warranted.

Excited leptons can always be pair produced via their weak and /or their electromagnetic charge. This is shown schematically in Fig. 46. Excited leptons can be also produced singly, via the magnetic coupling of an excited lepton with an ordinary lepton. This single production, however, is only of importance for the case of excited electrons where an additional t channel graph, as shown in Fig 47, considerably enhances the production cross section.

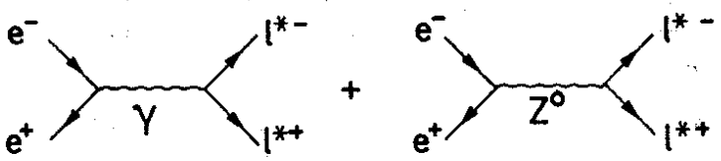

Fig 46: Pair production of excited leptons

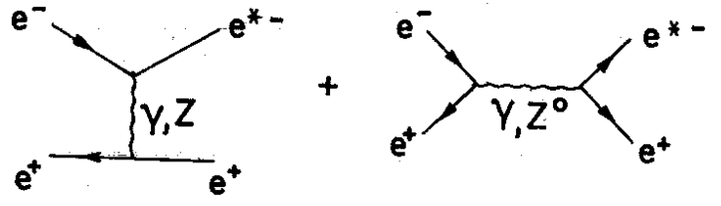

Fig 47: Single production of excited electrons

A detailed analysis of excited lepton production in e^+e^- collisions has been carried through recently by Hagiwara, Komamiya and Zeppenfeld [39], and we report here some of their conclusions. In this analysis it was assumed that the right handed excited leptons, L, sat in the same SU(2) xU(1) representation as the left handed leptons, l, and communicated with the ordinary leptons via a magnetic interaction of the type detailed by Cabibbo, Maiani and Srivastava [40]

$$L_{magn} = \frac{gf}{\Lambda}\left\{\bar{L}_R\,\sigma^{\mu\nu}\,\frac{\vec{\tau}}{2}\,l_L\,\partial_\mu\,\vec{W}_\nu\right\} + \frac{g'f'}{\Lambda}\left\{\bar{L}_R\,\sigma^{\mu\nu}\left(-\frac{1}{2}\right)l_L\;\partial_\mu\,B_\nu\right\} \qquad (V.7)$$

Here g and g' are the SU(2) and U(1) coupling constants, respectively, and $\vec{W}_\mu$ and B_μ are the relevant gauge fields. The parameters f and f' are arbitrary, but presumed to be of order unity, and Λ reflects the compositeness scale. (For practical applications one may set f=f'=1 and parametrize the

results as a function of the compositeness scale Λ). In the analysis of Ref [39] the excited leptons are allowed to have also an anomalous moment interaction with the gauge fields, so that

$$L_{int} = g\,\bar{L}\,\frac{\vec{\tau}}{2}\left[\gamma^\mu\,\vec{W}_\mu + \frac{K}{2m^*}\,\sigma^{\mu\nu}\,\partial_\mu\,\vec{W}_\nu\right]L + g'\bar{L}\left\{-\frac{1}{2}\right\}\left[\gamma^\mu\,B_\mu + \frac{K'}{2m^*}\,\sigma^{\mu\nu}\,\partial_\mu\,B_\nu\right]L \qquad (V.8)$$

Here m^* is the mass of the heavy lepton and K and K' are anomalous magnetic moments.

The production of excited electrons, and to some extent that of excited neutrinos, is enhanced due to the presence of the t channel vector boson exchange graph (see Fig 47). In fact, due to the singular photon exchange, the produced e^*'s prefer to go down the beam pipe. However, this is not a problem since one looks experimentally for the e^* decay products: $e^* \to e\gamma$. The resultant electron will be produced typically with a distribution [39]

$$\frac{d\Gamma}{d\cos\theta} \sim 1 + \cos\theta \qquad (V.9)$$

where θ is the angle to the electron beam direction. As can be seen in Fig 48, for values of Λ = 1 TeV (f=f'=1) the cross section for producing excited electrons is sizable ($\sigma \gtrsim 1$ pb) almost to the kinematical limit $m_{e^*} \lesssim 2E_b$. Excited neutrinos or muons are much less likely to be produced.

The production of excited leptons in pairs, via the graphs of Fig 46, is effective ($\sigma \gtrsim 1$ pb) for masses up to nearly $\sqrt{s}/2$. However, the actual magnitude of the cross section can be wildly affected by the presence of an anomalous magnetic moment term. As Fig 49 shows, the predictions for the pair production cross section can be an order of magnitude above or below those of the standard model if $K,K' \neq 0$. Obviously pair production is good for excited μ's and excited τ's, but single production is more effective for excited electrons.

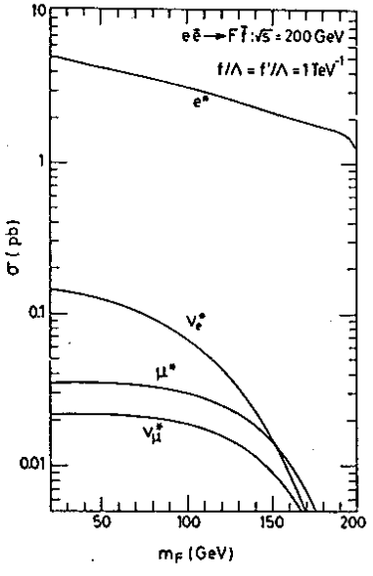

Fig 48: Production of excited leptons at LEP II energies, from Ref [39]

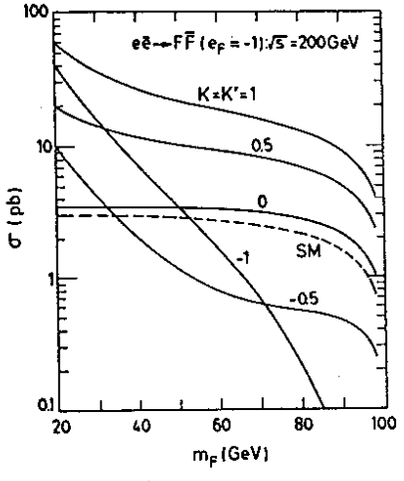

Fig 49: Effect of an anomalous magnetic moment on the pair production of excited leptons, from Ref [39]

V3: Exotic Leptons

As a last illustration of some of the phenomena which could arise if quarks and leptons where composite, we have considered a variety of exotic leptons and how they might manifest themselves at LEP II.

a) Leptoquarks: ϕ_{lq}

These are color triplet scalars with both quark and lepton number. The charge 2/3 leptoquark ϕ_{lq} (2/3) for all practical purposes will be pair produced like a u squark, $\tilde{u}$ (see [2] for a further discussion of supersymmetric partners of quarks and leptons). However, it has two distinct types of decay channels:

$$\phi_{lq}\ (2/3) \to \begin{cases} q(2/3)\bar{\nu} \\ q(-1/3)l^+ \end{cases} \qquad (V.10)$$

Only the first of these is analogous to the photino decay of the $\tilde{u}$: $\tilde{u} \to u\tilde{\gamma}$, giving rise to a jet plus missing energy. Typical signals for these exotic leptons are thus: 2 jets plus 2 leptons or 2 jets plus lepton plus missing energy, or 2 jets plus missing energy.

b)Vector Leptoquarks: V_{lq}

These objects are vector states which arise in certain models where W's are composite [41]. Although they are presumed to be much heavier than the W bosons, because if not they would upset the low energy phenomenology, they can nevertheless affect the process $e^+e^- \to q\bar{q}$ at LEP II. The exchange of a vector leptoquark in the t-channel, as shown in Fig 50, can interfere with the s-channel γ and Z^0 exchange, even if the vector leptoquark is quite heavy.

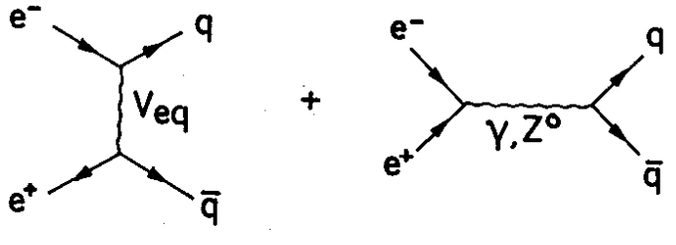

Fig 50: Contributions of vector leptoquarks to $e^+e^- \to q\bar{q}$ scattering

For example, taking the coupling of a V_{ed} leptoquark to be the same as that for the W

$$L_{int} = \frac{g_s}{2\sqrt{2}} \left[\bar{e}\, \gamma_\mu\, (1 - \gamma_5) d\ \ V^{\mu}_{ed} + \bar{d}\, \gamma_\mu\, (1 - \gamma_5) e\ \ V^{\dagger\mu}_{ed} \right] \qquad (V.11)$$

one can markedly modify the cross section for the process $e^+e^- \to \bar{d}d$ in the LEP II energy range, even if m_{ν_3} = 500-1000 GeV. This is shown pictorially in Fig 51.

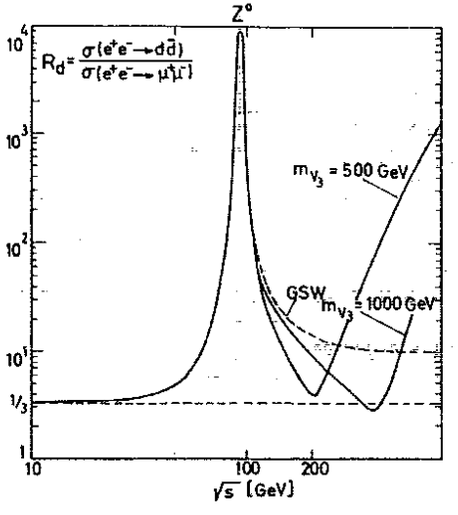

Fig 51: Effect of vector leptoquarks in the cross section of $e^+e^- \to d\bar{d}$

It is clear, therefore, that precision checks of the magnitude of the total hadronic cross section at LEP II can indicate the presence of such exotic objects. Note that these tests, and the effects here discussed, are not really very much different than those already examined in Sec V.1, connected with contact interactions.

c)Octet Leptons: l_8

These spin 1/2 objects, which carry octet color, sometimes arise in composite models where the constituents of leptons carry color [42]. They are unlikely to be light enough to be pair produced at LEP II. But if they are, they will give a spectacular jump in R:

$$\Delta R(l_8) = 8 \qquad (V.12)$$

preceded by many onia-like resonances. If they are heavy, they can still give additional contributions to the 2 jet cross section via the t-channel exchange of Fig 52, which is analogous to additional photon-photon production, in case excited electrons exist.

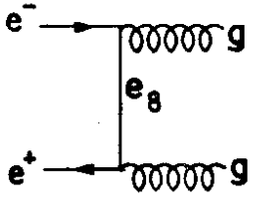

Fig 52: e_8 exchange graph leading to glue-glue production

The size of the e_8 contribution depends crucially on the magnitude of the magnetic coupling between an electron, a gluon, and e_8, which in analogy to the excited lepton-photon-electron coupling of Eq (V.7) can be parametrized via

$$L_{eff} = \frac{g_s}{2\Lambda} \bar{e}\, \sigma^{\mu\nu}\, (c + d\gamma_5) e^a_8\, F^a_{\mu\nu} + h.c. \qquad (V.13)$$

On general theoretical grounds L_{eff} should be chirality conserving, i.e. c = ±d. Otherwise (V.13) would induce a large anomalous contribution to the electron g-2. In the chirality conserving case, the differential cross section reads

$$\frac{d\sigma}{dt}(e^+e^- \to gg) = 8\pi\alpha_s^2 \left(\frac{c}{\Lambda}\right)^4 \frac{16tu}{s^2} \left[\left(\frac{t}{\frac{2}{m_{e_8}} - t} \right)^2 + \left(\frac{u}{\frac{2}{m_{e_8}} - u} \right)^2 \right] \qquad (V.14)$$

which agrees with Ref [48].

The resulting contribution to the total dijet cross section is shown in Fig 53 for two different choices of the parameter Λ.

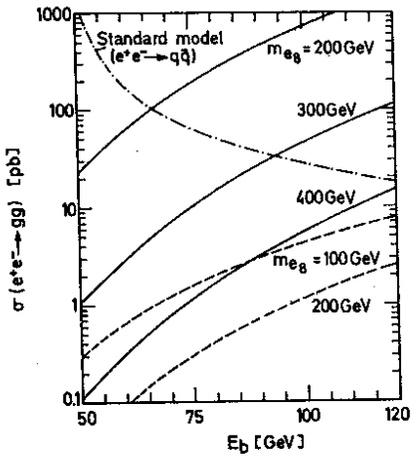

Fig S3: Two jet cross section produced by e_8 exchange

Fixing $c/\Lambda = (1\ \text{TeV})^{-1}$ it is orders of magnitude below the standard model $q\bar{q}$ background (dotted line) even for $m_{e_8} = 100$ and 200 GeV (dashed lines). If, however, the scale Λ/c is just m_{e_8}, then the effect of t-channel e_8 exchange is enormous, giving a cross section of near a nanobarn for $E_b = 100$ GeV and $m_{e_8} = 200$ GeV (see solid lines for $m_{e_8} = 200$, 300, 400 GeV). Because the cross section grows as s^3, changing m_{e_8} to a bigger value decreases the cross section as $(m_{e_8})^{-8}$. Clearly it is difficult to draw any direct conclusions from this exercise, except for being aware that if exotic leptons like e_8 exist, the total hadronic cross section at LEP II could be significantly affected.

VI: CONCLUDING REMARKS

We can summarize our findings concerning operating LEP at high energies in a concise way:

1) The physics interest for operating LEP at energies above the W^+W^- threshold is, to our minds, equal to if not greater than that of working in the Z^0 region.

2) LEP II is capable of pair producing objects (excited leptons, sparticles, new flavors, etc) with masses $m \lesssim E_b$ and singly producing objects of higher mass ($m_{e^*} \lesssim 2E_b$; $m_H \lesssim 2E_b - 100$ GeV). From this point of view, it is of interest to push E_b to the maximum possible value, although in certain cases (e.g. for the Higgs search) this may increase the background.

3) LEP II is uniquely suited to explore fundamental pieces of the SU(2) x U(1) gauge theory, like the three gauge coupling, the W mass, the production of longitudinal W bosons and the determination of the elements of the Kobayashi Maskawa matrix. For these purposes it is sufficient to operate LEP II around $E_b = 90$ GeV, although possible deviations from the standard model increase with E_b.

Acknowledgements

We are particulatly grateful to K.Hikasa, S.Komamiya, C.Matteuzzi, S.Ritz, P.Roudeau and S.L.Wu for their assistance in the preparation of this report. We would like to thank, furthermore, M.Hausser for her help in producing the many versions of this document and W.Knaut for drawing the many figures in the report.

Appendix A. Helicity Amplitudes for the Process $e^+e^- \to W^+W^-$

In this appendix we present all helicity amplitudes for the process

$$e(k,\sigma) + e^+(\bar{k},\bar{\sigma}) \to W^-(q,\lambda) + W^+(\bar{q},\bar{\lambda}) \qquad (A1)$$

as depicted in Fig. A1, calculated using the most general triple vector boson coupling consistent with Lorentz invariance. All the results in this and the next appendix are taken from Ref. [43].

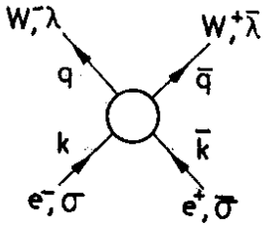

Fig A1: Schematic view of the process $e^+e^- \to W^+W^-$. The indices $\sigma,\bar{\sigma},\lambda,\bar{\lambda}$ denote helicities.

Fig 1, in the text, shows the three Feynman diagrams contributing to the process. The first two diagrams contain the triple vector boson vertices in which we are interested. There are, in general, seven independent form factors for each WWV (V = γ or Z) vertex when both W's are on mass shell and V couples to conserved currents. The Feynman rule for the WWV couplings, as depicted in Fig A2 can be expressed as follows: We choose

$$g_{WW\gamma} = e$$

$$g_{WWZ} = e \cot \theta_W \qquad (A2)$$

with e and θ_W denoting the proton charge and the Weinberg angle. Then the most general WWV vertex has the following form

$$\Gamma_V^{\alpha\beta\mu}(q,\bar{q},P) = (\bar{q}-q)^\mu \left[f_1^V g^{\alpha\beta} - \frac{f_2^V}{M_W^2} P^\alpha P^\beta + \frac{f_7^V}{M_W^2} \varepsilon^{\alpha\beta\rho\sigma} P_\rho (\bar{q}-q)_\sigma \right]$$

$$+ f_3^V (P^\beta g^{\mu\alpha} - P^\alpha g^{\mu\beta}) - i f_4^V (P^\beta g^{\mu\alpha} + P^\alpha g^{\mu\beta})$$

$$+ i f_5^V \varepsilon^{\mu\alpha\beta\rho} (\bar{q}-q)_\rho + f_6^V \varepsilon^{\mu\alpha\beta\rho} P_\rho \qquad (A3)$$

for V = γ and Z. Here the form factors f_i^V are in general dimensionless function of P^2,

$$f_i^V = f_i^V(P^2) \qquad (A4)$$

The phases are chosen in such a way that the form factors are real for $P^2 < 0$. The relations between these seven form factors and the nine (redundant) form factors of Gaemers and Gounaris [12] can be found in Ref [43].

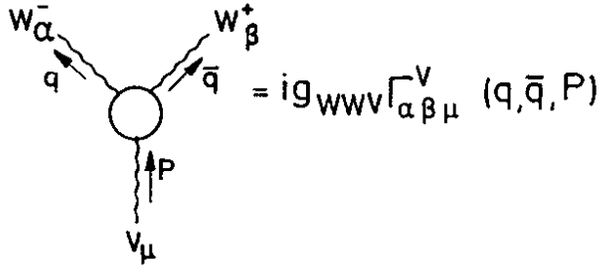

Fig A2: Feynman rule for the WWV vertex (V = γ or Z)

Electromagnetic gauge invariance constrains the WWγ couplings at $P^2 = 0$, i.e.

$$f_1^\gamma(P^2 = 0) = 1$$

$$f_i^\gamma(P^2 = 0) = 0 \text{ for } i = 4,5 \qquad (A6)$$

otherwise all the 14 couplings can take arbitrary complex values at LEP II energies, $P^2 \simeq (200\ \text{GeV})^2$. The appearances of certain of these imply violations of various discrete symmetries in the vector boson sector:

$$f_4^V,\ f_5^V \neq 0 \rightarrow \text{C violation}$$

$$f_3^V,\ f_6^V,\ f_7^V \neq 0 \rightarrow \text{P violation}$$

$$f_4^V,\ f_6^V,\ f_7^V \neq 0 \rightarrow \text{CP violation} \qquad \text{(A7)}$$

The first three couplings satisfy C and P invariance separately and are often parametrized as [44]

$$f_1^V\ (P^2 = 0) = g_1^V$$

$$f_2^V\ (P^2 = 0) = \lambda_V$$

$$f_3^V\ (P^2 = 0) = g_1^V + \kappa_V + \lambda_V \qquad \text{(A8)}$$

where $g_1^\gamma = 1$ is the electric charge of the W^+. The parameters κ_γ and λ_γ are related to the magnetic dipole and electric quadrupole moments of the W boson as follows:

$$\mu_W = \frac{e}{2M_W}\ (1 + \kappa_\gamma + \lambda_\gamma)$$

$$Q_W = -\frac{e}{2M_W^2}\ (\kappa_\gamma - \lambda_\gamma) \qquad \text{(A9)}$$

In the standard model, we expect

$$f_1^V\ (P^2) = 1 + O(\alpha)$$

$$f_3^V\ (P^2) = 2 + O(\alpha) \qquad \text{(A10)}$$

for both V = γ and Z. All the other form factors are either order α or higher, or absent. These constraints can also be expressed as

$$g_1^V = 1 + O(\alpha)$$

$$\kappa_V = 1 + O(\alpha)$$

$$\lambda_V = O(\alpha) \qquad \text{(A11)}$$

for both V = γ and Z at $P^2 = 0$.

Helicity amplitudes for the process $e^+e^- \rightarrow W^+W^-$ are a sum over three contributions, one from each of the diagrams shown in Fig 1 in the text

$$M(\sigma,\bar{\sigma},\lambda,\bar{\lambda}) = e^2\ [\ M^{(a)}\ (\Delta\sigma,\lambda,\bar{\lambda}) + M^{(b)}\ (\Delta\sigma,\lambda,\bar{\lambda}) + M^{(c)}\ (\Delta\sigma,\lambda,\bar{\lambda})\ ] \qquad \text{(A12)}$$

with $\Delta\sigma = \sigma - \bar{\sigma}$. Because in Fig 1 helicity is conserved on the electron lines, by the vector and axial vector interactions, Δσ takes only the two values ±1. In the e^+e^- center of mass frame the γ(a) and Z(b) contributions are related as follows

$$M^{(a)}\ (\pm,\lambda,\bar{\lambda}) = -\sqrt{2}\ \beta\ A_{\lambda\bar{\lambda}}^{\pm(\gamma)}(\cos\theta)$$

$$M^{(b)}\ (+,\lambda,\bar{\lambda}) = \sqrt{2}\ \beta\ \frac{s}{s-M_Z^2}\ A_{\lambda\bar{\lambda}}^{+(Z)}(\cos\theta)$$

$$M^{(b)}\ (-,\lambda,\bar{\lambda}) = \left(\sqrt{2}\ \beta - \frac{\beta}{\sqrt{2}\sin^2\theta_W}\right)\ \frac{s}{s-M_Z^2}\ A_{\lambda\bar{\lambda}}^{-(Z)}(\cos\theta) \qquad \text{(A13)}$$

where θ denotes the scattering angle between the e^- beam and the W^-, and $\beta = (1 - 4M_W^2/s)^{1/2}$ is the W velocity. All the coefficients $A_{\lambda\bar{\lambda}}^{\Delta\sigma(V)}(\cos\theta)$ are listed below (Δσ = + or −, V = γ or Z):

$$A^{\pm(V)}_{+0} = \pm\gamma(f^V_3 - if^V_4 + \beta f^V_5 + i\beta^{-1}f^V_6)\ (1 \pm \cos\theta)/2$$

$$A^{\pm(V)}_{0-} = \mp\gamma(f^V_3 + if^V_4 + \beta f^V_5 - i\beta^{-1}f^V_6)\ (1 \pm \cos\theta)/2$$

$$A^{\pm(V)}_{0+} = \mp\gamma(f^V_3 + if^V_4 - \beta f^V_5 + i\beta^{-1}f^V_6)\ (1 \mp \cos\theta)/2$$

$$A^{\pm(V)}_{-0} = \pm\gamma(f^V_3 - if^V_4 - \beta f^V_5 - i\beta^{-1}f^V_6)\ (1 \mp \cos\theta)/2$$

$$A^{\pm(V)}_{++} = \mp(f^V_1 + i\beta^{-1}f^V_6 + 4i\gamma^2\beta f^V_7)\ (\mp \frac{1}{\sqrt{2}} \sin\theta)$$

$$A^{\pm(V)}_{--} = \mp(f^V_1 - i\beta^{-1}f^V_6 - 4i\gamma^2\beta f^V_7)\ (\mp \frac{1}{\sqrt{2}} \sin\theta)$$

$$A^{\pm(V)}_{00} = \pm\gamma^2(-(1+\beta^2)f^V_1 + 4\gamma^2\beta^2 f^V_2 + 2f^V_3)\ (\mp \frac{1}{\sqrt{2}} \sin\theta) \qquad \text{(A14)}$$

where the factor γ in the amplitudes is $\gamma = E_W/M_W$. The θ dependent factors are essentially the d functions [45], $d^1_{\Delta\sigma,\Delta\lambda}$, with $\Delta\lambda = \lambda - \bar{\lambda}$.

The neutrino exchange (c) contributions are absent when $\Delta\sigma = +1$ due to the V-A coupling.

$$M^{(c)}\ (+,\lambda,\bar{\lambda}) = 0 \qquad \text{(A15)}$$

The surviving nine other amplitudes can be expressed as

$$M^{(c)}\ (-,\lambda,\bar{\lambda}) = \frac{1}{\sqrt{2}\sin^2\theta_W} C_{\lambda\bar{\lambda}}\ (\cos\theta) \qquad \text{(A16)}$$

where

$$C_{\pm\mp} = \mp\sqrt{2}\ D\ (1\mp\cos\theta)\sin\theta$$

$$C_{0-} = -C_{+0} = \frac{1}{\beta}\left[\gamma - \frac{1+\beta}{\gamma} D\right] (1-\cos\theta)$$

$$C_{0+} = -C_{-0} = \frac{1}{\beta}\left[\gamma - \frac{1-\beta}{\gamma} D\right] (1+\cos\theta)$$

$$C_{++} = C_{--} = \frac{1}{\beta}\left[1 - \frac{1}{\gamma^2} D\right] (\frac{1}{\sqrt{2}} \sin\theta)$$

$$C_{00} = -\frac{2}{\beta}\left[\gamma^2 - \frac{1}{\gamma^2} D\right] (\frac{1}{\sqrt{2}} \sin\theta) \qquad \text{(A17)}$$

Here D denotes the neutrino propagator factor

$$D = [1 + \beta^2 - 2\beta\cos\theta]^{-1} \qquad \text{(A18)}$$

This completes the description of all the amplitudes. For the standard model couplings of Eq (A10), one can see the cancellation of the singular terms proportional to γ and γ^2 clearly. In particular, the singular terms in the photon exchange are cancelled by part of the singular terms in the Z exchange contribution, and the rest is cancelled by the neutrino exchange contribution. Furthermore Eqs (A13) show clearly the smallness of the $\Delta\sigma = +1$ cross sections in the standard model, due to cancellation at $s \gg m_Z^2$ of $M^{(a)}$ with $M^{(b)}$.

If all the form factors are real, Im $f^V_i(P^2) = 0$, then the following relation holds in general

$$M(\sigma,\bar{\sigma},\lambda,\bar{\lambda}) = M(-\bar{\sigma},-\sigma,-\bar{\lambda},-\lambda)^*\ (-1)^{\lambda+\bar{\lambda}} \qquad \text{(A19)}$$

which is just a consequence of CPT invariance under the absence of absorptive parts. Hence a violation of the relation (A19) directly measures final state interactions, irrespective of the existence of an anomalous triple vector boson coupling. CP violation can be detected by testing the relation

$$M(\sigma,\bar{\sigma},\lambda,\bar{\lambda}) = M(-\bar{\sigma},-\sigma,-\bar{\lambda},-\lambda)\ (-1)^{\lambda+\bar{\lambda}} \qquad \text{(A20)}$$

which is a consequence of CP invariance, with no extra assumptions. A more detailed phenomenological study of tests of anomalous couplings and of symmetries at LEP II, is contained in Ref [43].

Appendix B. Angular Distribution of W_T and W_L in the Standard Model

In this appendix we present analytic expressions for the angular distribution of polarized W bosons in the standard model. For the standard model couplings of Eq (A10), the amplitudes presented in the previous appendix simplify significantly. In particular the relation

$$A_{\lambda\bar{\lambda}}^{\Delta\sigma(\gamma)}(\cos\theta) = A_{\lambda\bar{\lambda}}^{\Delta\sigma(Z)}(\cos\theta) \tag{B1}$$

which is valid for all helicity combinations, help simplify the sum of the γ and Z exchange contributions.

For the scattering of a right-handed electron and a left-handed positron, $\Delta\sigma = +1$, only the γ and Z exchange diagrams contribute. Let us write

$$M(\sigma,\bar{\sigma},\lambda,\bar{\lambda}) = e^2 M_{\lambda\bar{\lambda}}^{\Delta\sigma} \tag{B2}$$

and list all the 7 nonvanishing amplitudes for $M_{\lambda\bar{\lambda}}^{+}$:

$$M_{\pm 0}^{+} = -M_{0\mp}^{+} = \sqrt{2}\,\beta\gamma\,\frac{M_Z^2}{s - M_Z^2}\,(1 \pm \cos\theta)$$

$$M_{\pm\pm}^{+} = \beta\,\frac{M_Z^2}{s - M_Z^2}\,\sin\theta$$

$$M_{00}^{+} = -\beta(2\gamma^2 + 1)\,\frac{M_Z^2}{s - M_Z^2}\,\sin\theta \tag{B3}$$

We can immediately see that all these amplitudes, except M_{00}^{+}, vanish for $s \gg m_z^2$. Furthermore, near threshold, the P-wave factor β suppresses the cross section. Numerically, the sum of all $\Delta\sigma = +1$ contributions is always less than a few percent of the total cross section at LEP II.

More interesting is the scattering of a left-handed electron and a right-handed positron, the $\Delta\sigma = -1$ contributions. Amplitudes with double helicity

flip $\lambda-\bar{\lambda} = \pm 2$ do not receive contributions from s-channel vector boson exchange and are trivial;

$$M_{\pm\mp}^{-} = \mp\,\frac{1}{\sin^2\theta_W}\,D(1\mp\cos\theta)\sin\theta \tag{B4}$$

where D is the neutrino propagator factor of Eq (A18). For the remaining 7 amplitudes, all three diagrams contribute:

$$M_{\pm 0}^{-} = -M_{0\mp}^{-} = -\sqrt{2}\left[\frac{\beta\gamma M_Z^2}{s - M_Z^2} - \frac{1}{2\sin^2\theta_W}\left(\frac{\beta\gamma s}{s - M_Z^2} - \frac{\gamma}{\beta} + \frac{1 \pm \beta}{\beta\gamma}\,D\right)\right](1\mp\cos\theta)$$

$$M_{\pm\pm}^{-} = \left[\frac{\beta M_Z^2}{s - M_Z^2} - \frac{1}{2\sin^2\theta_W}\left(\frac{\beta s}{s - M_Z^2} - \frac{1}{\beta} + \frac{1}{\beta\gamma^2}\,D\right)\right]\sin\theta$$

$$M_{00}^{-} = -\left[\frac{\beta(2\gamma^2 + 1)M_Z^2}{s - M_Z^2} - \frac{1}{2\sin^2\theta_W}\left(\frac{\beta(2\gamma^2 + 1)s}{s - M_Z^2} - \frac{2\gamma^2}{\beta} + \frac{2}{\beta\gamma^2}\,D\right)\right]\sin\theta \tag{B5}$$

Here cancellations of all the terms which lead to tree unitary violation (terms with γ and γ^2) are manifest. The 16 helicity amplitudes (B3) - (B5) are the only ones which are non vanishing in the standard model, at tree level, provided the electron mass is neglected.

The cross sections with definite helicity for all the particles involved are expressed as

$$\frac{d\sigma(\sigma,\bar{\sigma},\lambda,\bar{\lambda})}{d\cos\theta} = \frac{\beta}{32\pi s}\left|M(\sigma,\bar{\sigma},\lambda,\bar{\lambda})\right|^2$$

$$= \frac{\pi\alpha^2\beta}{2s}\left|M_{\lambda\bar{\lambda}}^{\Delta\sigma}\right|^2 \tag{B6}$$

with $\alpha = e^2/4\pi$. Cross sections averaged over initial beam polarizations are

then expressed as

$$\frac{d\sigma_{\lambda\bar{\lambda}}}{d\cos\theta} = \frac{\pi\alpha^2\beta}{8s} \sum_{\Delta\sigma=\pm} \left|M_{\lambda\bar{\lambda}}^{\Delta\sigma}\right|^2 \qquad (B7)$$

By inserting Eqs (B3) to (B5), we find for the nine W^+W^- helicity combinations the following formulas

$$\frac{d\sigma_{\pm\mp}}{d\cos\theta} = \frac{\pi\alpha^2\beta}{8x_W^2 s} D^2 (1\mp\cos\theta)^2 \sin^2\theta$$

$$\frac{d\sigma_{\pm 0}}{d\cos\theta} = \frac{d\sigma_{0\mp}}{d\cos\theta} = \frac{\pi\alpha^2\beta}{4s}\left\{\left[\frac{\beta\gamma M_Z^2}{s-M_Z^2}\right]^2 (1\pm\cos\theta)^2 + \left[\frac{\beta\gamma M_Z^2}{s-M_Z^2} - \frac{1}{2x_W}\left(\frac{\beta\gamma s}{s-M_Z^2} - \frac{\gamma}{\beta} + \frac{1\pm\beta}{\beta\gamma} D\right)\right]^2 (1\mp\cos\theta)^2\right\}$$

$$\frac{d\sigma_{\pm\pm}}{d\cos\theta} = \frac{\pi\alpha^2\beta}{8s}\left\{\left[\frac{\beta M_Z^2}{s - M_Z^2}\right]^2 + \left[\frac{\beta M_Z^2}{s - M_Z^2} - \frac{1}{2x_W}\left(\frac{\beta s}{s - M_Z^2} - \frac{1}{\beta} + \frac{1}{\beta\gamma^2} D\right)\right]^2\right\} \sin^2\theta$$

$$\frac{d\sigma_{00}}{d\cos\theta} = \frac{\pi\alpha^2\beta}{8s}\left\{\left[\frac{\beta(2\gamma^2+1)M_Z^2}{s - M_Z^2}\right]^2 + \left[\frac{\beta(2\gamma^2+1)M_Z^2}{s - M_Z^2} - \frac{1}{2x_W}\left(\frac{\beta(2\gamma^2+1)s}{s - M_Z^2} - \frac{2\gamma^2}{\beta} + \frac{2}{\beta\gamma^2} D\right)\right]^2\right\} \sin^2\theta$$

where $x_W = \sin^2\theta_W$. (B6)

If we do not distinguish between the two transversly polarized W's, then we have

$$\frac{d\sigma_{TT}}{d\cos\theta} = \sum_{\lambda=\pm}\sum_{\bar{\lambda}=\pm} \frac{d\sigma_{\lambda\bar{\lambda}}}{d\cos\theta} \qquad \frac{d\sigma_{TL}}{d\cos\theta} = \sum_{\lambda=\pm} \frac{d\sigma_{\lambda 0}}{d\cos\theta}$$

$$\frac{d\sigma_{LT}}{d\cos\theta} = \sum_{\bar{\lambda}=\pm} \frac{d\sigma_{0\bar{\lambda}}}{d\cos\theta} \qquad \frac{d\sigma_{LL}}{d\cos\theta} = \frac{d\sigma_{00}}{d\cos\theta} \qquad (B7)$$

If we do not even distinguish W^+ from W^- , then we can define inclusive distributions for transversly and longitudinally polarized W's:

$$\frac{d\sigma_T}{d\cos\theta} = \left(\frac{d\sigma_{TT}}{dz} + \frac{d\sigma_{TL}}{dz}\right)_{z=\cos\theta} + \left(\frac{d\sigma_{TT}}{dz} + \frac{d\sigma_{LT}}{dz}\right)_{z=-\cos\theta}$$

$$\frac{d\sigma_L}{d\cos\theta} = \left(\frac{d\sigma_{LL}}{dz} + \frac{d\sigma_{LT}}{dz}\right)_{z=\cos\theta} + \left(\frac{d\sigma_{LL}}{dz} + \frac{d\sigma_{TL}}{dz}\right)_{z=-\cos\theta} \qquad (B8)$$

These distributions (B7) and (B8) have been shown in the text.

Appendix C. W mass measurement using their decays into $l\nu_e$ or jet-jet

P.Roudeau
LAL, Orsay, France

The W decays mainly in 2 jets; these jets, in case of leptonic decays, contain only one particle (e, μ) or very few particles (τ). In the reaction $e^+e^- \to W^+W^-$, at about 100 GeV beam energy, the jets emitted in the final state are energetic and well separated from their neighbours. For most of the LEP experiments, the use of finely segmented electromagnetic and hadronic calorimeters allows the measurement of individual photon or neutral hadron energies. Charged tracks are accurately reconstructed in large volume tracking devices.

When gathering, with a jet algorithm [46], the W decay products, some particles are lost. The jet reconstruction algorithm can attribute a few of them to the other W or they can have crossed an inefficient or a non-equipped region of the detector. Some particles belonging to the other W are conversely added to the one we are studying. Most of these particles have a small momentum and thus a rather isotropic angular distribution.

Our ability to reconstruct correctly the jet directions remains essentially unaltered whereas the jet energies determination can be not so accurate. These considerations are developed in a more quantitative way in [47]. At LEP, the knowledge of the W energy which is simply equal to the energy of the beam allows to recover a good accuracy on the W mass determination.

1) W mass reconstruction in jet-jet decays.

We consider for the moment only four jets events and attribute to a W decay the 2 jets combination whose energy is the closest to the beam energy. The 2-jets mass is shown in Fig 30, in the text. A peak appears centered at 81.5 GeV with a FWHM of ~ 4.7 GeV. The nominal W mass used in the simulation is 83.2 GeV and the W width is supposed to be zero.

If we rescale the reconstructed mass value by the ratio E_{beam}/E_W, where E_W is equal to the observed W energy, we obtain the mass distribution shown in

Fig 31, in the text. The peak is now centered at 83.115 GeV ± 12 MeV and the width is 1.769 GeV ± 46 MeV. (The statistics represents 2700 W decays). The systematic mass shift is less than 100 MeV and may be related to the effect of particle losses in a given hadronization scheme.

The effect of the electron beam radiation has been studied, the previous peak remains with an additional tail extending towards higher masses. This behaviour can be exactly simulated and corrected using a Monte Carlo simulation.

2) W mass reconstruction in the decay $W \to l\nu_e$.

We consider now events having 3 reconstructed jets and we demand that the jet with the smallest number of particles - slim jet - does not contain more than 4 particles. The lepton from the W decay is identified as the electron or muon having the maximum energy inside this jet. The remaining hadrons inside the slim jet are attributed to the other two jets. With this procedure we can form the 2-jets mass as before. The statistics is reduced by about 3.4 compared to the previous case but events are cleaner, and apart from the contribution of τ decays, which can be essentially removed by a more careful analysis, all the reconstructed particles from the 2 jets decay are correctly attributed to the W, as shown in Fig C1.

Having imposed that the 2-jet energy is equal to the beam energy we have determined the 4-vector of the ν emitted in the other W decay by requiring energy momentum conservation. The mass of the neutrino-lepton system is shown in Fig C2, for which we have also required the 2 jet mass of the other W to be around the nominal W mass within ± 2 GeV. This mass distribution is well centered around the W mass but broader than in the previous cases because it requires the measurement of the W's common direction, from the reconstruction of the decay of the other W.

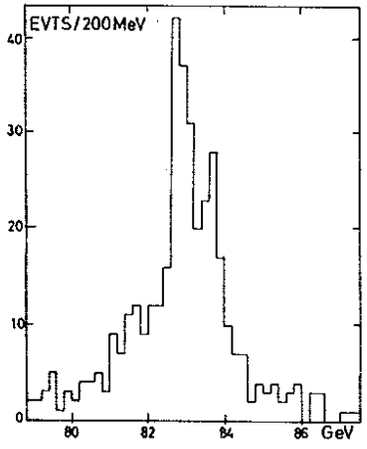

Fig C1: W mass when the other W decays leptonically

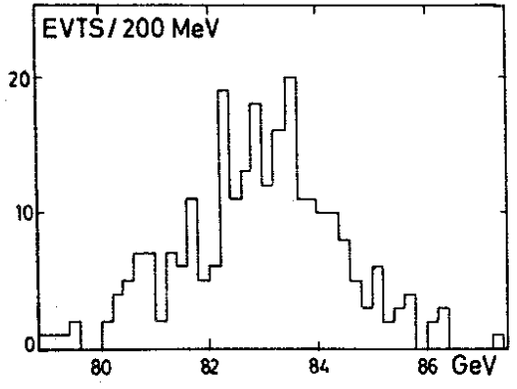

Fig C2: Mass of a W decaying into $l\nu_e$, when the other W decays into hadrons

References

[1] P.Bernard, H.Lengeler and E.Picasso, LEP note S24
CERN/EF/RF 85-1

[2] H.Baer et al, these proceedings

[3] S.L.Glashow, Nucl. Phys. 22 (1961) 579;
S.Weinberg, Phys. Rev. Lett. 19 (1967) 1264
A.Salam, in Elementary Particle Theory ed. N.Svartholm
(Almquist and Wiksell, Stockholm 1968)

[4] W.Alles, Ch.Boyer and A.J.Buras, Nucl. Phys. B119 (1977) 125;
O.P.Sushkov, V.V.Flambaum and I.B.Khriplovich,
Sov. J. Nucl. Phys. 20 (1975) 537;
see also Ref [8]

[5] M.Lemoine and M.Veltman, Nucl. Phys. B164 (1980) 445

[6] R.Philippe, Phys. Rev. D26 (1982) 1588

[7] R.Kleiss, private communication

[8] R.W.Brown and K.O.Mikaelian, Phys. Rev. D19 (1979) 922;
W.J.Sterling, Proceedings of the 5th Tropical Workshop on
Proton-Antiproton Colliders Physics, ed. M.Greco (World
Scientific, Singapore, 1985)

[9] E.Eichten, I.Hinchliffe, K.Lane, C.Quigg, Rev. Mod. Phys. 56
(1984) 579

[10] The three gauge coupling γWW can probably be also quite well
tested in hadronic colliders. See, for a discussion, R.W.Brown,
D.Sahdev and K.O.Mikaelian, Phys. Rev. D20 (1979) 1164;
J.Cortés, K.Hagiwara and F.Herzog, Desy report 85-132.

[11] N.Cabibbo and R.Gatto, Phys. Rev. 124 (1961) 1577

[12] K.J.F.Gaemers and G.J.Gounaris, Z. Phys. C1 (1979) 259

[13] R.Casalbuoni, S. de Curtis, D.Dominici and R.Gatto, Phys. Lett. 155B (1985) 95;
M.S.Chanowitz and M.K.Gaillard, Phys. Lett. 142B (1984) 85

[14] There exist a number of studies in the literature of the effect of nonstandard gauge couplings for the process $e^+e^- \to W^+W^-$. Some recent examples are C.L.Bilchak and J.D.Stroughair, Phys. Rev. D30 (1984) 1881; T.G.Rizzo, Phys. Rev. 32 (1985) 43; J.Maalampi, D.Schildknecht and K.H.Schwarzer, Bielefeld preprint BI-TP 85/20

[15] D.Dicus and K.Kalliampur, Phys. Rev. D32 (1985) 35

[16] A.Bilal and M.Davier, ALEPH note MAY 1985

[17] A.Sirlin, Phys. Rev. D22 (1980) 971

[18] W.J.Marciano and A.Sirlin, Phys. Rev. D22 (1980) 2695;
ibd. D29 (1984) 945;
M.Consoli, L.Maiani and S.Lo Presti, Nucl. Phys. B223 (1983) 474

[19] A.Sirlin, Phys. Rev. D29 (1984) 89

[20] W.J.Marciano, Phys. Rev. D20 (1979) 274

[21] See for example L. di Lella, Proceedings of the 1985 Europhysics Conference on High Energy Physics, Bari, Italy ed L.Nitti and G.Preparata (Laterza, Bari 1985)

[22] G.Altarelli et al., these proceedings

[23] M.Bassetti and B.Montague, LEP 390 report

[24] M.Consoli, L.Maiani and S.LoPresti, Ref [18]

[25] V.A.Kovalchuk, M.P.Rekalo and I.V.Stoletnii
DESY L-Trans-295 (1984)

[26] M.Kobayashi and T.Maskawa, Prog. Theor. Phys. 49 (1973) 652

[27] See for example J.Ellis, M.K.Gaillard, G.Girardi and P.Sorba Ann. Rev. Nucl. Part. Sci. 32 (1982) 443;
G.Altarelli, Proceedings of the XII International Winter Meeting on Fundamental Physics, Santillana del Mar, Spain (1984)

[28] G.Arnison et al, Phys. Lett. 147B (1984) 493

[29] K.Kleinknecht in Flavor Mixing in Weak Interactions ed by L.L.Chau (Plenum Press, N.Y. 1984)

[30] C.Matteuzzi, private communication

[31] I.Hinchliffe in Elementary Particle Physics and Future Facilities ed by R.Donaldson, R.Gustafson and F.Paige (Snowmass 1982)

[32] For a discussion see R.D.Peccei in Proceedings of the 5^{th} Tropical Workshop on Proton-Antiproton Collider Physics, ed. M.Greco (World Scientific, Singapore, 1985)

[33] B.L.Ioffe and V.A.Khoze, Sov. J. Part. Nucl. 9 (1978) 50;
B.W.Lee, C.Quigg and H.B.Thacker, Phys Rev D16 (1977) 1519;
R.L.Kelly and T.Shimada, Phys. Rev. D23 (1981) 1940

[34] W.Buchmüller et al, these proceedings

[35] For a recent review, see for example, W.Buchmüller, in Proceedings of the XXIV Schadming School, CERN TH-4189/85

[36] E.Eichten, K.Lane and M.Peskin, Phys. Rev. Lett. 50 (1983) 811

[37] S.Komamiya, Proceedings of the International Symposium on Lepton Photon Interactions at High Energies, Kyoto, August 1985

[38] S.M.Barr, Phys. Rev. Lett. 55 (1985) 2778;
E.Cohen, J.Ellis, K.Enqvist and D.V.Nanopolous, CERN TH-4222;
L.S.Durkin and P.Langacker UPR-0287T
V.Barger, N.G.Deshpande and K.Whisnant, Phys. Rev. Lett. 56 (1986) 30

[39] K.Hagiwara, S.Komamiya and D.Zeppenfeld, Z. Phys. C29 (1985) 115

[40] N.Cabbibo, L.Maiani and Y.Srivastava, Phys. Lett. 139B (1984) 459

[41] A prototype model is that of L.Abbott and E.Fahri, Phys. Lett. 101B (1981) 69; Nucl. Phys. 189B (1981) 547;
see also B.Schrempp and F.Schrempp, Nucl. Phys. B231 (1984) 109

[42] H.Fritzsch and G.Mandelbaum, Phys. Lett. 102B (1981) 319;
for a discussion, see also, H.Harari in Proceedings of the 5^{th} Tropical Workshop on Proton-Antiproton Collider Physics, ed. M.Greco (World Scientific, Singapore 1985)

[43] K.Hagiwara, K.Hikasa, R.D.Peccei and D.Zeppenfeld,
DESY report, in preparation

[44] T.D.Lee and C.N.Yang, Phys. Rev. 128 (1962) 885;
H.Aronson, Phys. Rev. 186 (1969) 1434;
K.J.Kim and Y.-S.Tsai, Phys. Rev. D7 (1973) 3710

[45] M.E.Rose, Elementary Theory of Angular Momentum
(John Wiley, New York 1957)

[46] T.Sjöstrand, Computer Physics Comm. 28 (1983) 229

[47] P.Roudeau, Delphi note 85-49 Phys. 5

[48] F.M.Renard, Montpellier preprint PM 85-20